10-28-2015

Lignin-derived thermosetting vinyl ester resins for high performance applications

Daniel Rogers
Rowan University

LIGNIN-DERIVED THERMOSETTING VINYL ESTER RESINS FOR HIGH PERFORMANCE APPLICATIONS

by
Daniel P. Rogers

A Thesis

Submitted to the
Department of Chemical Engineering
College of Engineering
In partial fulfillment of the requirement
For the degree of
Master of Science in Chemical Engineering
at
Rowan University
October 2, 2015

Thesis Chair: Joseph F. Stanzione, III

Dedications

For Mom and Dad

Acknowledgments

I would like thank my advisor, Dr. Stanzione, for his guidance and unrelenting support throughout my graduate work. Dr. Stanzione has given me the opportunity to develop as both a leader and engineer, which is something that will help me throughout the rest of my career. He has been a true inspiration and I would not be the person I am today without him. Dr. Stanzione has taught me key concepts in chemical engineering, green engineering, and polymer science, and has introduced me to many scientists and engineers within his network. Without Dr. Stanzione, this thesis would not have been possible. In addition, I would like to thank the rest of the chemical engineering faculty at Rowan University, especially Dr. Hesketh and Dr. Staehle, for serving as advisors and mentors throughout my undergraduate chemical engineering career.

I would also like to thank Alex Bassett and Brandon Hummer, who have provided me with indispensable help and support throughout my graduate research. Without them, this thesis would not have been completed as quickly as it was. Moreover, I would like to acknowledge Dr. John La Scala for his support and technical advice throughout my research. In addition, I would like to thank the Army Research Labs for their financial support via Cooperative Agreement W911NF-14-2-0086.

I am grateful for the encouragement from my family and friends throughout my career at Rowan University. I especially would like to thank my mother, Bette Rogers, and father, Gary Rogers, for their unwavering support and motivation throughout my childhood and educational journey.

Abstract

Daniel P. Rogers

LIGNIN-DERIVED THERMOSETTING VINYL ESTER RESINS FOR HIGH PERFORMANCE APPLICATIONS

2015

Joseph F. Stanzione, III

Master of Science in Chemical Engineering

Vinyl ester (VE) resins are utilized to produce polymer matrix composites for use in a wide range of applications due to possessing relatively high moduli, strengths, and glass transition temperatures while maintaining low weight and cost. VE resins often contain high concentrations of a petroleum-based reactive diluent (RD), such as styrene. Many of the commonly used RDs have been designated as hazardous air pollutants, potential carcinogens, and volatile organic compounds. Renewable VE resins and RDs with similar performance to petroleum-based RDs are desired to potentially mitigate the aforementioned hazards as well as to facilitate the transition from petrochemical feedstocks to bio-based feedstocks. Lignin, which is an abundant renewable resource with a high aromatic content, has the potential to replace petrochemical feedstocks for VE resins and RDs. Lignin is produced in excess of $50x10^6$ tons annually as low value fuel for energy recovery, yet has the potential to produce high value chemicals and polymer precursors. In this work, a review of the literature was conducted in order to create multiple lignin-derived bio-oil mimics that were functionalized and subsequently polymerized to make high performance thermosetting plastics. In addition, lignin-derived compounds were investigated for use as RDs in a VE resin system to potentially reduce or eliminate the need for petrol derived RDs. The thermo-mechanical properties of all plastics were investigated via dynamic mechanical analysis and various structure property relationships are proposed.

Table of Contents

Abstract v

List of Figures ix

List of Tables xi

Chapter 1: Introduction 1

1.1 Overview and Organization 1

1.2 Vinyl Ester Resins 2

1.3 Lignin 5

1.3.1 Delignification 8

1.3.2 Lignin Applications 10

1.3.3 Lignin Depolymerization 11

1.4 Summary 13

Chapter 2: Characterization Techniques 15

2.1 Introduction 15

2.2 Nuclear Magnetic Resonance (NMR) 15

2.3 Fourier Transform Infrared Spectroscopy (FTIR) 17

2.4 Gel Permeation Chromatography (GPC) 19

2.5 Dynamic Mechanical Analysis (DMA) 20

Chapter 3: Development and Characterization of Lignin-derived Bio-oil Mimic Resins for High Performance Applications 24

3.1 Introduction 24

3.2 Experimental 25

3.2.1 Materials 25

3.2.2 Lignin-derived Bio-oil Compositions 26

Table of Contents (Continued)

3.2.3 Synthesis of MLMCs 31

3.2.4 Resin Curing 34

3.2.5 Extent of Cure 34

3.2.6 Polymer Properties 34

3.3 Results and Discussion 35

3.3.1 Resin Characterization 35

3.3.2 Extent of Cure 42

3.3.3 Polymer Properties 44

3.4 Conclusions 52

Chapter 4: Methacrylated Lignin Model Compounds for use as Reactive Diluents in Vinyl Ester Resins 53

4.1 Introduction 53

4.2 Experimental 54

4.2.1 Materials 54

4.2.2 Synthesis of Vinyl Ester Resin 54

4.2.3 Synthesis of MLMCs 58

4.2.4 Resin Curing 60

4.2.5 Extent of Cure 61

4.2.6 Polymer Properties 62

4.3 Results and Discussion 62

4.3.1 Resin Characterization 62

4.3.2 Extent of Cure 65

4.3.3 Polymer Properties 67

Table of Contents (Continued)

4.4 Conclusions....78

Chapter 5: Conclusions and Recommendations....80

5.1 Conclusions....80

5.2 Recommendations....81

References....83

Appendix A: ^{1}H NMR Spectra....91

Appendix B: GPC Traces of Pure MLMCs....95

Appendix C: GPC Standard Curve....98

List of Figures

Figure Page

Figure 1. Structure of (a) methacrylate and (b) acrylate vinyl ester functional groups....3

Figure 2. Example unsaturated polyester resin (UPE).[19]....4

Figure 3. VE828 synthesis via the reaction between DGEBA and methacrylic acid, adapted from La Scala *et al*.[22]....4

Figure 4. Chemical structure of monolignols: *p*-coumaryl alcohol R1=R2=H / coniferyl alcohol R1=OMe, R2=H / sinapyl alcohol R1=R2=OMe, adapted from Chakr *et al*.[27].....6

Figure 5. General structure of lignin, which was adapted from Jia *et al*.[29]....7

Figure 6. Example DMA thermogram that relates storage modulus and loss modulus to temperature....22

Figure 7. Phenolic chemicals that were utilized in creating the bio-oils presented in this thesis....27

Figure 8. Esterification reaction used to methacrylate lignin-derived bio-oil mimics....32

Figure 9. ^{1}H NMR spectra of MBO1 after aqueous washing. The peak labels correspond to the methacrylated compound numbers in *Figure 8* 36

Figure 10. ^{1}H NMR spectra of MBO2 after aqueous washing. The peak labels correspond to the methacrylated compound numbers in *Figure 8* 37

Figure 11. ^{1}H NMR spectra of MBO3 after aqueous washing. The peak labels correspond to the methacrylated compound numbers in *Figure 8* 38

Figure 12. GPC trace for MBO1, MBO2, MBO3, and polystyrene standards. The number average molecular weights for the polystyrene (PS) standard are: a - 532,000 Da, b - 59.300 Da, c - 8650 Da, and d - 492 Da 40

Figure 13. The GPC traces of MBO1, MBO2, and MBO3 are shown. The predicted retention time of methacrylated 4-methylcatechol (the highest MW methacrylated lignin model compound) is given by the vertical line at a retention time of 28.3 minutes. The peaks represented by * are hypothesized to be “oligomers”....41

Figure 14. Photos of cured (a) MBO1, (b) MBO2, and (c) MBO3....42

Figure 15. Near-IR Extent of Cure for MBO1, MBO2, and MBO3. The methacrylate C=C bond peaks are labeled * and the =CH2 peaks are labeled ** 43

Figure 16. DMA results for MBO1, MBO2, and MBO3 45

Figure 17. Intramolecular cyclization of methacrylated catechol, adapted from Ohya *et al*.[81] 49

Figure 18. Tan δ results for MBO1, MBO2, and MBO3 as a function of temperature. 51

Figure 19. Synthesis of VE828 from DGEBA and methacrylic acid in the presence of AMC-2 catalyst at 80-90 °C, adapted from La Scala *et al.*[22]. 55

Figure 20. Mid-IR spectra of Epon and VE828 with * representing hydroxyl groups and ** representing carbonyl groups 56

Figure 21. GPC trace for VE828 and Epon 828, with * representing n=1 and ** representing n=0 57

Figure 22. Reaction of lignin model compounds with methacrylic anhydride to produce methacrylated lignin model compound monomers 59

Figure 23. Pictures of cured (a) 1:1VE828:PM, (b) 1:1 VE828:MG, (c) 1:1 VE828:M4PG 65

Figure 24. Near-IR spectra for 1:1 blends of VE828 and purified PM, MG, and M4PG. The methacrylate C=C bond peaks are labeled * and the =CH2 peaks are labeled ** 66

Figure 25. VE828 blends made with impure reactive diluents and styrene for commercial comparison, adapted from Stanzione *et al*.[72] 69

Figure 26. VE828 blends made with pure reactive diluents and styrene for commercial comparison 71

Figure 27. The tan δ of VE828 resins diluted with impure MLMCs and styrene is shown as function of temperature, adapted from Stanzione *et al*.[72] 77

Figure 28. The tan δ of VE828 resins diluted with pure MLMCs and styrene is shown as function of temperature 78

List of Tables

Table Page

Table 1. Estimated percentage of linkages in softwood protolignin, adapted from Chakar *et al.*[27] 8

Table 2. Delignification pyrolysis conditions for the studies utilized in this thesis 13

Table 3. Average weight percent, count, and objective number for the single aromatic molecules used to generate BO1 29

Table 4. Average weight percent, count, and objective number for the single aromatic molecules used to generate BO2 29

Table 5. Concentrations of all lignin-derived bio-oil mimics 31

Table 6. Extent of Cure for MBO1, MBO2, and MBO3 44

Table 7. Thermo-mechanical properties of MBO1, MBO2, and MBO3 46

Table 8. Experimentally determined molecular weights of VE828 on the bases of GPC and ^{1}H NMR 58

Table 9. Purity of MLMCs, on the basis of ^{1}H NMR, after aqueous wash purification[72] 63

Table 10. Purity of MLMCs, on the basis of ^{1}H NMR, after aqueous wash and flash chromatography purification 64

Table 11. Extent of cure of pure and impure VE828:RD resins 67

Table 12. Bio-based content of VE828-based thermosets 68

Table 13. Thermo-mechanical properties of VE828 blends with impure MLMCs and styrene, adapted from Stanzione *et al*[72] 70

Table 14. Thermo-mechanical properties of VE828 blends with pure MLMCs and styrene 72

Table 15. VE828:RD weight ratio to molar ratio conversion 74

Chapter 1

Introduction

1.1 Overview and Organization

Building a sustainable world is one of the most challenging and important projects of the 21st century. The drive for a sustainable future has been fueled by the unintended environmental and economic consequences caused by rapidly growing societies and economies. One of the most promising prospects for a sustainable future is through the production of energy, fuels, and chemicals from biological resources in next generation biorefineries. In these biorefineries, petrochemical feedstocks are replaced with biomass, which is renewable, to produce the same or similar chemicals. Biorefineries are likely to be regional, were local resources are used as a feedstock.[1] In addition, biorefineries would provide a framework for the United States to produce industrial chemicals and polymers independently without the need for imports from other countries.[1] In 2005, the U.S. Department of Energy and Department of Agriculture predicted that biomass would be used as a feedstock in the production of 25 % of all chemical and materials by 2030.[2]

In order to ensure the profitability and success of biorefineries, all biomass components (cellulose, hemicellulose, and lignin) need to be utilized.[3] A large hurdle for the success of these biorefineries is the use of lignin, which is a highly aromatic bio-polymer that has received considerable attention in academia/industry for the production of aromatic specialty chemicals, polymers, and composites.[1, 3-11] Polymer and composite materials are traditionally derived from petrol feedstocks; however, there have been recent advances in the degradation and use of lignin-derived compounds for

thermosetting epoxy and vinyl ester resins (VERs) applications.[3, 7, 12-14] This thesis investigates the use of lignin as a sustainable feedstock for the production of vinyl ester thermosetting resins. In subsequent Chapter 1 sections, background information relevant to the work presented in this thesis is provided. A general introduction to thermosetting VERs is given, followed by an introduction to lignin. Motivation for the use of lignin as a feedstock for VERs is given along with information on lignin applications, delignification, and depolymerization. Lastly, a brief summary on the work presented in this thesis is provided.

1.2 Vinyl Ester Resins

In 2008, the United States produced 58 million metric tons of polymers, with the largest majority being attributed to plastics (84 %).[15] In addition, production of polymers consumed 20 % of all the industrial organic chemicals produced in the U.S.[15] Polymers can be classified into two distinct categories: thermoplastics and thermosets.[15-17] Thermoplastic polymers will melt upon heating, producing a free flowing polymer network, and can be thermally processed. Thermosets have covalent bonds that connect polymer chains to produce intricate three dimensional polymer networks with infinite molecular weights. Thermosets do not melt upon heating, but are subject to decomposition at high temperatures and are insoluble in all solvents. Thermosetting resins account for approximately 25 % of all plastics produced and can be used to make plastics, elastomers, coatings, adhesives, inks, paints, cements, and composites.[17]

A large class of thermosetting polymers is VERs, which are the focus of this thesis. VERs are used in a variety of composite applications and typically provide high

thermal stability, moduli (>2 GPa at 25°C), strength, glass transition temperature (T_g, >120 °C), chemical resistance, and low water absorption.[18, 19] Due to the high performance characteristics and low processing costs, these resins are often used in the construction, marine, and transportation industries.[20] Specifically, VERs are widely used in solvent storage tanks, pipes, and swimming pools.[19] Uncured VERs are characterized by having an ester group with a carbon-carbon double bond that is located at the end of the polymer chain.[21] Acrylate and methacrylate vinyl ester function groups are shown in *Figure 1*.

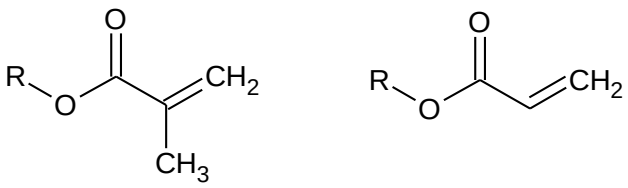

(a) (b)

Figure 1. Structure of (a) methacrylate and (b) acrylate vinyl ester functional groups.

VERs were first commercialized by Shell Chemical Co. in 1965, with Dow Chemical Co. following shortly thereafter.[19] It is common for VERs to replace UPE resins because of their increased chemical resistance.[19] UPE resins typically have unreacted carbo- carbon double bonds, hydroxyl groups, and carboxylic acids after curing that are prone to hydrolytic, oxidation, and halogenation reactions, whilst VERs only have ester linkages at the end of the polymer chain.[19] The chemical structure of an UPE resin is shown in *Figure 2*.[19]

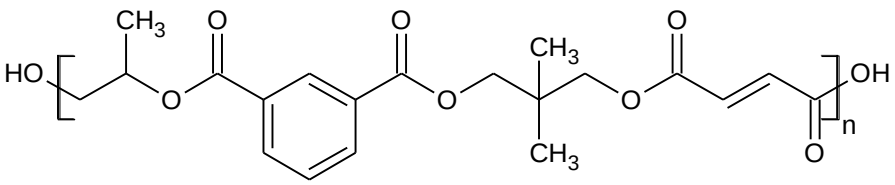

Figure 2. Example unsaturated polyester resin (UPE).[19]

VERs can be synthesized by the reaction of an epoxy resin with either acrylic or methacrylic acid.[17-19, 22] An example of this is the synthesis of a commercial VER, VE828, through the methacrylation of diglycidyl ether of Bisphenol A (DGEBA), which is shown in *Figure 3*.[22]

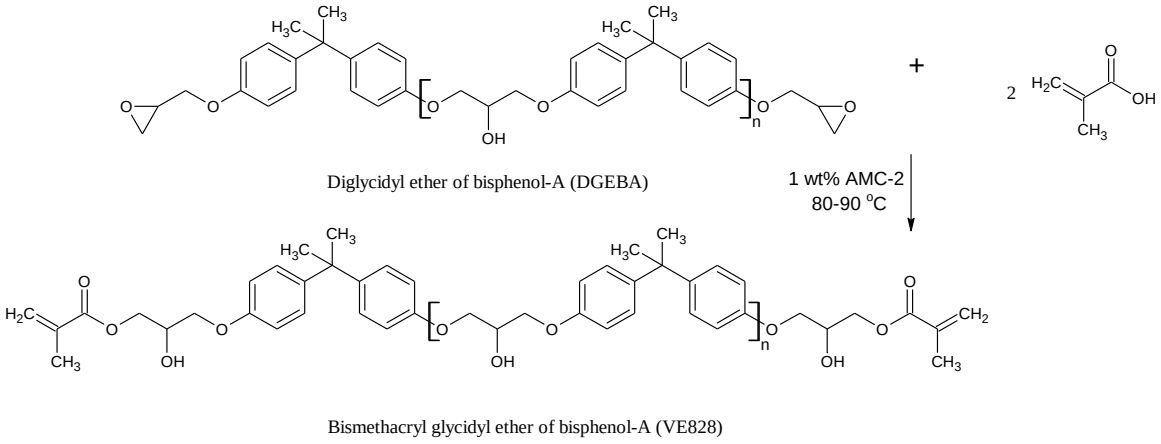

Figure 3. VE828 synthesis via the reaction between DGEBA and methacrylic acid, adapted from La Scala *et al.*[22]

VE resins typically undergo bulk-free radical polymerization that is initiated with an organic peroxide or hydroperoxide; however, due to the high viscosity of VERs (long polymer backbone), a reactive diluent (RD), such as styrene, vinyl toluene, or methyl

methacrylate, is used to reduce the viscosity of the resin.[19, 22] Typically, the viscosity of VERs is reduced to 200-1000 cP prior to processing.[19] Upon curing, the RD and VER react together to form an intricate thermosetting polymer network.[17] Most RDs used in VERs are non-renewable; however, it is possible that, when functionalized, lignin-derived phenolic compounds can be used as renewable substitutes.[12] Using bio-based material to develop renewable RDs would increase the total sustainable content of the cured vinyl ester plastic. In addition, lignin derivatives have the potential to produce low viscosity VERs, which have the potential to replace the need for many of the petrol-derived VERs that are in production today.[12]

1.3 Lignin

Lignin is a highly cross-linked, aromatic, amorphous biopolymer that has been considered one of the most important bioresources for the production of sustainable fuels and industrial chemicals in the 21st century. Produced in excess of 2×10^{10} tons annually within the biosphere, lignin is the second most abundant biopolymer, behind cellulose.[5, 7, 23, 24] Due to the fact that lignin is rich in aromaticity, it has the potential to produce high value chemicals and polymer precursors and has received considerable attention from industry and academia as a possible renewable feedstock that can reduce global dependence on fossil fuels.[1, 3, 4, 25, 26] In addition, lignin is produced in excess of $50x10^6$ tons annually as a waste byproduct of paper mills, where most is burned as a low value fuel for energy production.[3] Due to the aromaticity of lignin, along with the fact that it is produced in large quantities industrially, lignin is an attractive feedstock for chemical applications.

Lignin is found within the cell walls of vascular plants and, on a dry basis, accounts for 15 to 36 % of woody biomass.[3, 27] It is formed via a radical based biosynthesis of *p*-coumaryl alcohol, guaiacyl, and syringyl.[4, 25] These chemicals, which are referred to as monolignols, are shown in *Figure 4*.[27]

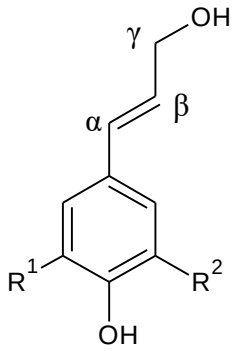

Figure 4. Chemical structure of monolignols: *p*-coumaryl alcohol R_1=R_2=H / coniferyl alcohol R_1=OMe, R_2=H / sinapyl alcohol R_1=R_2=OMe, adapted from Chakr *et al*.[27]

Due to the enzyme initiated dehydrogenative polymerization mechanism, lignin has an amorphous structure in contrast to the repeating macromolecular structures of cellulose and hemicellulose.[1] There are many compositional models for the structure of lignin that can be found in the literature; however, it is accepted that lignin does not have a universally defined structure.[28] A general chemical structure of lignin is shown in *Figure 5*, which was adapted from Jia *et al*.[29]

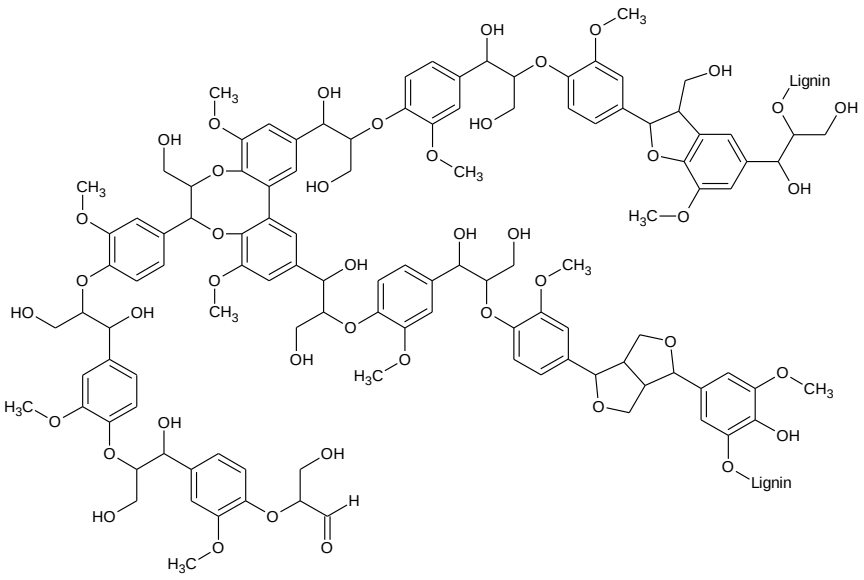

Figure 5. General structure of lignin, which was adapted from Jia *et al*.[29]

Prior to separation from cellulose and hemicellulose, lignin is referred to as protolignin.[1] The term lignin is normally used for isolated protolignin, which has chemical structure different than that of protolignin.[1, 4, 28] The most common phenylpropane linkage in lignin is β-O-4. The percentage of linkages in softwood protolignin are shown in Table 1, which was adapted from Chakar et al.[27]

Table 1.

Estimated percentage of linkages in softwood protolignin, adapted from Chakar et al.[27]

Linkage	Percentage of Total Linkages
β-O-4	45-50
α-O-4	6-8
β-5	9-12
5-5	18-25
4-O-5	4-8
β-1	7-10
β-β	3

The exact chemical structure of lignin depends of a number of factors, some of which include the type of biomass, environmental conditions in which the protolignin was synthesized, and the type of delignification process used for separation.[4, 27] For example, the structure of lignin is highly dependent on the polysaccharide gel within the cell wall.[4] In addition, different types of biomass will have a varying concentration of *p*-coumaryl alcohol, guaiacyl, and syringyl units.[25]

1.3.1 Delignification. The process of separating lignin from cellulose and hemicellulose in biomass is referred to as delignification. The first delignification process was designed in 1874 and utilized calcium-based sulfite liquors[1]. With the invention of the Tomlinson recovery furnace in the 1930s, the Kraft process was widely adopted, which as of 2004, accounted for the production of 95 % of all industrial lignin.[1, 7] The purpose of the Kraft pulping process is to remove an adequate amount of lignin to produce a pulp that can be used to manufacture paper products.[27] The Kraft process provides a notable improvement over the calcium-based sulfite pulp process due to the fact that cations and sulfur compounds can be recovered and reused.[1, 27] In addition,

99 % of lignin that is produced in the Kraft process is burned as a low value fuel for energy recovery.[1]

The Kraft process utilizes an aqueous solution of sodium hydroxide and sodium sulfide, which is referred to as white liquor.[1, 27] Wood chips are introduced into the white liquor and the bulk solution is heated and allowed to equilibrate at 150 to 170 °C for two hours.[27] During this period, the hydroxide and hydrosulfide anions will cleave phenylpropane linkages and produce hydroxyl groups, which increase the solubility of lignin in the alkali liquor.[27] The resulting alkali liquor after the lignin extraction is referred to as black liquor.[1, 27] The black liquor is typically evaporated down and burned for energy recovery.[1] Residual lignin is removed through subsequent bleaching techniques, as further alkali-based reactions will begin to significantly cleave carbohydrate bonds after a two hour time period.[27] Lignin can be recovered from the black liquor by acidification with carbon dioxide and sulfuric acid; however, Kraft lignin typically has a low, yet significant, sulfur content.[27] There are several studies that utilize Kraft lignin as a feedstock for the production of single aromatic chemicals.[13, 26, 30-35] With improved technology, it may be possible to develop a cost effective process to recover and refine lignin from the black liquor in Kraft processes.[1]

Other methods of delignification include organosolv processes, which are solvent-based. These processes utilize organic solvents and are characterized by higher efficiency, fewer byproducts, reduced emissions, and reduced capital costs when compared to alkali processes.[28] In addition, organosolv lignins are considered higher quality than Kraft lignins due to an increased concentration of phenyl hydroxyls and carbonyls, a decreased T_g that allows for easier thermal processing, and an absence of

sulfur.[36] Examples of organosolv processes include Alcell (ethanol), Acetosolv (acetic acid), Formacell (formic acid), and Organocell (methanol).[1] It is likely that next generation biorefineries will utilize organosolv delignification processes in order to produce lignins of higher quality as a feedstock for chemical applications. The ability to produce high quality lignins makes organosolv biorefineries economically viable.[37] In addition to chemical and solvent delignification processes, enzymatic delignification also has been investigated in academia.[1, 38-40] It is estimated that enzymatic delignification has the potential to be both efficient and environmentally friendly; however, significant progress is necessary in order for enzymatic delignification to be used to produce lignin on an industrial scale.[38]

1.3.2 Lignin applications. As stated previously, the majority of lignin is burned as a low value energy source in the pulp and paper industry. However, with advances in lignin delignification technologies sparked by increased academic and industrial research, it is likely that there will be many profitable alternatives to using lignin as an energy source. In a 2008 review by Derek Steward, many applications for lignin-derived compounds were proposed, which span areas that include phenolic resins, epoxies, adhesives, and polyolefins.[41] High volume and low market value applications include biofuels and soil, asphalt, and fuel additives that would sell for approximately $100 per ton.[3] Low volume and high market value applications include resins, plastics, and specialty chemicals that could potentially sell for $11,000 per ton.[3] Currently, the cost of low grade lignin (Kraft black liquor) is about $50 per ton, while high purity lignin (organosolv) costs upwards of $800 per ton.[3] An example of a specialty chemical product that is derived from lignin is vanillin. The majority of vanillin was produced

from lignin derivatives in the 1980s, but due to the large amount of waste produced in the vanillin to lignin process, only 15 % of vanillin is produced in this manner (2004).[34] Today, the bio-refinement company Borreegaard is the only company to produce lignin-derived vanillin on an industrial scale. In the near future, vanillin may be produced from Kraft lignin in an integrated process that can be implemented into paper mills.[35]

1.3.3 Lignin depolymerization. In order to ensure the success of next generation lignocellulose biorefineries, it is essential that lignin be used for a higher value application than low value energy production. Due to the aromaticity of protolignin, lignin has the potential to become a feedstock for high value specialty chemicals and polymers when selectively depolymerized into single-aromatic or multi-aromatic compounds. One of the major barriers in the use of lignin as a chemicals and polymers feedstock is due to the cost effectiveness of depolymerization technologies. The heterogeneity of lignin, in addition to the variance in chemical structures of different types of lignin (due to the type of biomass and process used in delignification), make it difficult to depolymerize lignin on an industrial scale.[3] Technological developments in lignin depolymerization are beginning to emerge that will make lignin processing into specialty chemicals and polymers profitable.[3]

Lignin can be selectively broken down by a variety of methods, which include pyrolytic, catalytic, enzymatic, oxidative, and fractionation techniques.[1, 3, 26, 30, 33, 38, 39, 42-46] The most prominent lignin depolymerization method is pyrolysis, where lignin is heated to high temperatures (typically 400 K to 1000 K) at atmospheric pressure in the absence of oxygen. The main products of lignin pyrolysis are char, condensable gasses, and non-condensable gasses, all of which have the potential for profitable

applications.[3, 26] It was proposed by De Wild *et al*. that current, state of the art, industrial sized biomass pyrolysis reactors are not capable of effectively depolymerizing lignin.[3] However, the Energy Research Center of the Netherlands (ECN) has made recent advances and developed a lignin bio-refinery approach (LIBRA) process that is capable of pyrolyzing lignin continuously on a pilot scale.[3] Typical organic yields from this process range from 22 % to 29 % of dry lignin weight and typically contains 6-7 % of monomeric phenols.[3] Another challenge in the degradation of lignin is the cost effective refinement of the organic phase, often referred to as a lignin-derived bio-oil.[3] Technologies such as distillation, membrane separation, ultracentrifugation, and extraction may be needed in order to separate oligomers from single aromatic compounds.[3]

In recent years, numerous studies have been conducted on the chemical composition of the condensable gases organic phase.[26, 30-33, 42-56] With recent advances in pyrolysis-gas chromatography-mass spectroscopy systems (Py-GC-MS), new light has been shed on the resulting lignin-derived bio-oil compositions for many different pyrolysis conditions and lignin types. Table 2 shows the pyrolysis conditions and lignin types for the lignin-derived bio-oil compositional studies used in this thesis.[26, 30-33]

Table 2.

Delignification pyrolysis conditions for the studies utilized in this thesis

Source	Wood Types	Delignification Process	Fast Pyrolysis Catalyst	Fast Pyrolysis Temp. (°C)
[30]	Information Not Given	Kraft	HZSM-5, FCC, Olivine	470-560
[26]	Softwood	Kraft	MW Thermal	627-967
[33]	Pine, Milled Wood	Kraft	Information Not Given	300-500
[32]	Alcell lignin, Asian lignin	Organosolv & Soda Pulping Process	Information Not Given	400-800
[31]	Softwood, Hardwood	Kraft	Information Not Given	575-700

Information on why these studies were chosen can be found in Chapter 3 of this thesis. It should be noted that there are several other studies that investigate the composition of lignin-derived bio-oils.[42, 43, 45-56]

1.4 Summary

In order to ensure the success and profitability of next generation sustainable bio-refineries, all components of lignocellulosic biomass need to be utilized towards high value applications. The aromatic structure of lignin makes for a versatile feedstock that can be used to produce a variety of specialty chemicals, polymers, and fuels. Recent advances in delignification and lignin depolymerization technologies have opened the door for application based research geared towards producing sustainable, environmentally friendly, and profitable products.

Chapter 3 is an extension of the work done by Dr. Stanzione, whereby methacrylated lignin bio-oil mimcs are utilized to produce sustainable thermosetting VERs. A review of the literature was conducted in order to generate multiple lignin-

derived bio oil mimics. The mimics were functionalized and polymerized as a whole in order to investigate the use of lignin-derived bio-oils without the need for extensive separations. A follow-up to this research is presented in Chapter 4, where individual lignin model compounds were functionalized and utilized as RDs in a commercial VER, VE828. Chapter 5 concludes the work presented in this thesis and provides recommendations for future work.

Chapter 2

Characterization Techniques

2.1 Introduction

The fundamental characterization techniques that were used in this thesis are discussed. The principles on which these techniques are based on, as well as relevant governing equations, are given. Specific information on how these instruments and techniques were utilized in experimental setups can be found in subsequent chapters.

2.2 Nuclear Magnetic Resonance (NMR)

Nuclear magnetic resonance (NMR) spectroscopy was developed in the late 1950s and has since become one of the most important and useful tools to confirm or determine the structure of organic molecules. To do this, NMR spectroscopy takes advantage of radio-frequency radiation by nuclei and the nuclear transition from one energy level to another.[57] It can be used to determine the number and connectivity of hydrogen and carbon atoms through ^{1}H-NMR spectroscopy and ^{13}C-NMR spectroscopy, respectively.[57]

An atomic nucleus with an odd mass number and/or an odd atomic number has a nuclear magnetic moment, which is a result of its nuclear spin. Each nucleus has a specific spin state that is determined by the nuclear spin quantum number, I, based on the equation $2I + 1$. For example, ^{1}H, ^{2}H, ^{12}C, and ^{13}C have nuclear spin quantum numbers of ½, 1, 0, and ½, respectively, with $2I+1$ spin states.[57, 58] A nucleus that has a nuclear spin quantum number of zero, for example ^{12}C, has only one spin state and is therefore inactive in NMR spectroscopy.

In the absence of a magnetic field, the orientation of each nucleus is random. When a magnetic field, B_0, is applied to a nucleus, it will orient itself in one of its $2I + 1$ spin states, with the higher and lower energy state designated alpha (α) and beta (β), respectively. The lower energy state is when the nucleus is aligned with the magnetic field and the higher energy state is when the nucleus is aligned against the magnetic field.[57]

The energy difference between the two energy states is proportional to the strength of the magnetic field, as shown in Equation 1,

$$\Delta E = \gamma \frac{h}{2\pi} B_0 \tag{1}$$

where γ is the gyromagnetic ratio (26,753 sec^{-1} for ^1H) and h is Plank's constant.[59] If a nucleus is irradiated with energy equal to the energy difference between the α and β energy states, the nucleus will can absorb a photon and flip into a different energy state. When the nucleus changes energy states, it is considered to be in resonance. The energy of a photon is shown in Equation 2,

$$\Delta E = h\nu \tag{2}$$

where ν is the frequency of its electromagnetic wave. Equations 1 and 2 can be combined to determine the frequency of the electromagnetic waves, which is also referred to as the resonance frequency of the nucleus (Equation 3).[59]

$$\nu = \frac{1}{2\pi} \gamma B_0 \tag{3}$$

The number of protons in α and β energy states is given by the Boltzmann distribution as shown in Equation 4,

$$\frac{N_\beta}{N_\alpha} = e^{\frac{-h\nu}{kT}} \quad (4)$$

where N represents the number of protons in the α or β energy state, k is Boltzmann's constant, and T is absolute temperature. [57, 59]

The electrons on each nuclei and neighboring nuclei generate an induced magnetic field that shields B_0.[59] The magnetic field at the nucleus of an atom is less than B_0; therefore, a stronger magnetic field is necessary in order for resonance to occur at a specific frequency. Depending on electrons in the nearby environment, a nucleus will be shielded by different amounts. For example, a proton bonded to an oxygen atom will be less shielded than a proton bonded to a carbon atom due to the electronegativity of the oxygen atom.[59] By measuring the strength of the magnetic field that is required for resonance, information on the number protons and the structure of the molecule can be determined.[59] In a NMR spectrum, nuclear resonance absorption is plotted versus chemical shift (ppm). The chemical shift is defined as the shift downfield form tetramethylsilane (Hz) divided by the total spectrometer frequency (MHz).[59]

Tetramethylsilane (TMS) is used as a reference compound because the protons on the methyl groups are highly shielded when compared to carbon based molecules. As a result, most organic compounds will appear downfield of the TMS peak. Molecules are often dissolved in deuterated solvents that have one spin state and are therefore inactive in NMR spectroscopy. Common solvents are dimethylsulfoxide, chloroform, and water.[59]

2.3 Fourier Transform Infrared Spectroscopy (FTIR)

Fourier transform infrared spectroscopy is a powerful tool that can be used to detect the type of chemical bonds present within a molecule. The IR spectrum is

considered one of the more characteristic spectrums and is divided into three general regions; far IR, mid IR, and near IR.[59, 60] The wavelengths of these regions are 400-10 cm^{-1}, 4000-400 cm^{-1}, and 14285-4000 cm^{-1}, respectively.[59, 60] In order to obtain this spectrum, IR radiation is irradiated through the sample and the resulting frequencies that are absorbed are detected and measured at a given energy.[57, 60] The energy at a given frequency is due to the vibrational frequency of molecular bonds and groups within a molecule.

When a molecule is irradiated with IR radiation, the rotational and vibrational energy levels are changed.[59] In addition, different frequencies correspond to energy level changes within different functional groups. The change in energy level of each functional group can be quantified and detected by the spectrophotometric system. Energy level changes normally range from 2 to 10 kcal/mol.[60] In order for a functional group to absorb IR radiation, it must have a dipole moment.[57] A change in the dipole moment of a function group due to IR radiation causes stretching and bending vibrational frequencies. There are many different types of vibrational modes, which include stretching and bending. A change in bond length is classified as stretching and a change in bond angle is referred to as bending. Chlorine, oxygen, and nitrogen are examples of species that are inactive in IR spectroscopy due to the absence of a dipole moment.[59]

Traditional IR spectroscopy utilizes dispersive technology, whereby IR radiation is dispersed at all frequencies and only one frequency can be measured at a time.[60] As a result, extensive scan times are necessary to obtain an IR spectrum. FTIR utilizes an interferogram pattern, where a beam splitter is used to split the IR source into two parts, one of which is reflected and the other is transmitted.[60] For mid-IR systems, a KBr

beam splitter that is coated with germanium is used.[59, 60] The two beams travel different distances, which result in constructive or destructive interference patterns when recombined. The energy at each IR frequency is detected and quantified, resulting in an interferogram. The interferogram is in the time domain, so a Fourier transform is applied for conversion into the frequency domain to provide an interpretable spectra.[59, 60] In this thesis, near-IR spectroscopy was utilized to determine the extent of cure of all vinyl ester plastics. For the resins presented in this work, the near-IR region normally has fewer overlapping peaks than the mid-IR region. In addition, the near-IR peaks are of a lower intensity, which allows for the use of thicker samples.[59] Specifics on extent of cure calculations can be found in the experimental sections of Chapters 3 and 4.

2.4 Gel Permeation Chromatography (GPC)

Gel permeation chromatography is a useful analytical tool in the polymer engineering field that can be used to determine the average molecular weight and molecular weight distribution of a polymer mixture.[61, 62] GPC is a form of size exclusion chromatography, where molecules are separated based upon their size when dissolved in solvent.[61, 62] It is common for polymers to swell differently when dissolved; therefore, it is necessary to report what standards and solvent were used in this technique. In GPC, the dissolved polymer, typically at a concentration of 2 mg/mL, is forced through a packed column at a flow rate of 1-2 mL/min.[61] The packed column is filled with highly porous beads with a pore diameter in the range of $10\text{-}10^7$ Å.[61, 62] A typical packing material is a styrene-divinylbenzene cross-linked gel. As the dissolved polymer flows through the packing material, smaller molecular chained molecules are hindered by the pores in the packing material. Larger molecules are too big to fit into

these pores and are therefore not hindered. Because of this, the larger molecules will elute through the column first, followed by the smaller molecules.[62] Many different detectors are utilized in order to monitor the concentration of polymer in the eluent, such as refractive index, ultraviolet light, or laser light scattering.[61] In this dissertation, a refractive index detector was used. The intensity of the refractive index can be plotted as a function of elution time to generate a chromatogram. This chromatogram can be compared to a known molecular weight distribution of a standard such as polystyrene, for example.

2.5 Dynamic Mechanical Analysis (DMA)

Dynamic mechanical analysis (DMA) is a widely used rheological tool that measures the viscoelastic properties of materials as a function of time, temperature, and frequency. Generally, a sinusoidal force is applied to a sample and the response to the force is measured. The applied sinusoidal force is a function of amplitude (ε^0), frequency (ω), and time (t), and is given by Equation 5.[63, 64]

$$\varepsilon = \varepsilon^0 \sin(\omega t) \tag{5}$$

In viscoelastic materials, such as polymers and composites, there is a time delay, expressed as a phase angle (δ), between the applied sinusoidal strain force to the resulting stress response (σ). The stress response is given by Equation 6.[64]

$$\sigma = \sigma^0 \cos(\omega t + \delta) \tag{6}$$

The stress response can be expressed by in-phase and out-of-phase moduli, which are given by the real and imaginary parts of the stress response.[63] The in-phase storage modulus (E') is a measure of stored elastic energy during deformation and the out-of-

phase loss modulus (E'') is a measure of the heat lost during deformation.[64, 65] The equations for storage and loss modulus are given by Equations 7 and 8, respectively.

$$E' = \frac{\sigma^0}{\varepsilon^0}\cos(\delta) \tag{7}$$

$$E'' = \frac{\sigma^0}{\varepsilon^0}\sin(\delta) \tag{8}$$

The complex Young's modulus of viscoelastic materials is given by Equation 9, which is a sum of E' and E''.[65]

$$E^* = E' + iE'' = \sqrt{E'^2 + E''^2} \tag{9}$$

The storage modulus is often divided by the loss modulus to produce the loss tangent, which is given by Equation 10.[65]

$$\frac{E''}{E'} = \tan(\delta) \tag{10}$$

An example of a DMA thermogram that relates storage modulus and loss modulus to temperature is shown in *Figure 6*.

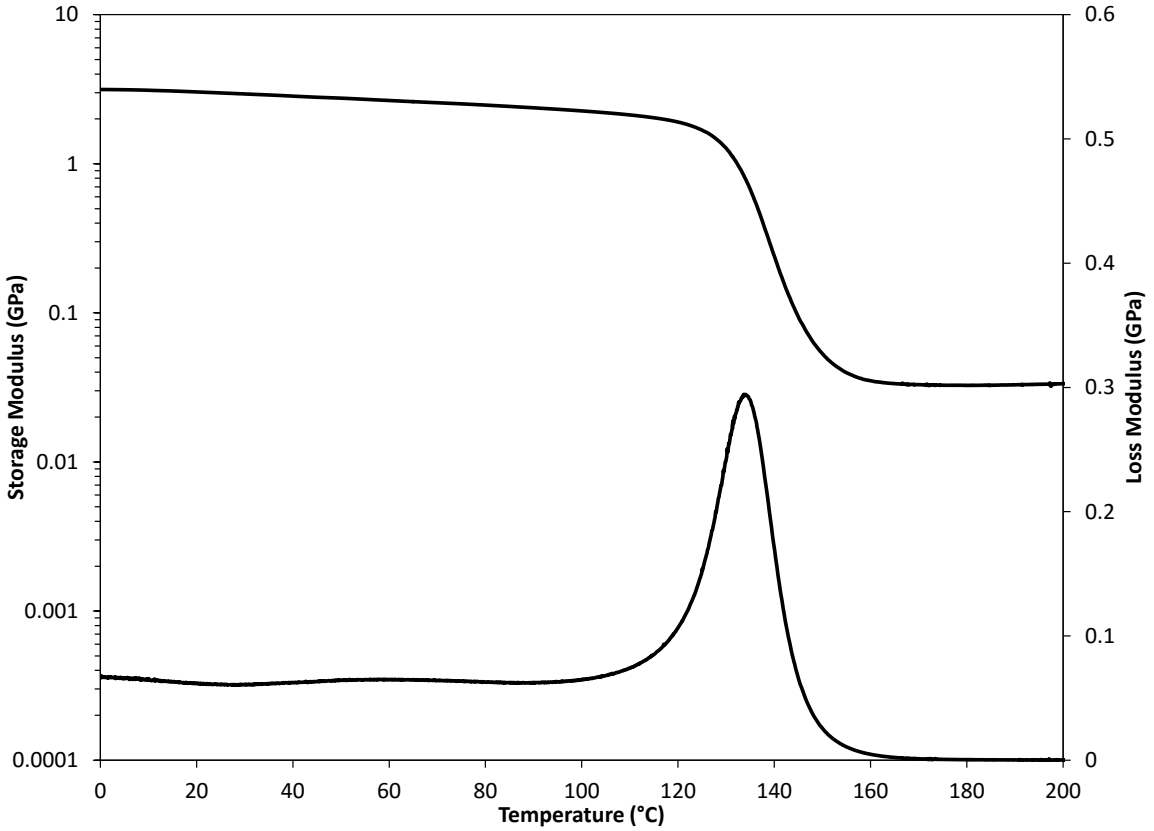

Figure 6. Example DMA thermogram that relates storage modulus and loss modulus to temperature.

There are three general regions that a cross-linked amorphous polymer can exhibit[65]. The first region is the glassy region, where the polymer is glass like and brittle. The storage modulus in the glassy region is normally at a maximum due to strong intramolecular interactions between polymer chains.[65] After subsequent heating, the polymer enters the glass transition region, which is defined as the onset of coordinated bulk molecular movement of polymer chains.[65] The glass transition temperature can be defined as the temperature at which the loss modulus or loss tangent peaks.[65] The loss modulus normally peaks at lower temperatures that then loss tangent; therefore, the loss

modulus is used as a conservative glass transition temperature. During the glass transition, the storage modulus normally decreases by a factor of 1000. The final region is the rubbery region, where the storage modulus remains relatively constant.[65] Linear amorphous polymers will exhibit additional rubbery flow regions and liquid flow regions.[65]

Chapter 3

Development and Characterization of Lignin-derived Bio-oil Mimic Resins for High Performance Applications

3.1 Introduction

In future biorefineries, lignocellulosic black liquor waste from the pulp and paper industry could be broken down into individual phenolic compounds through pyrolytic processes; however, extensive separation processes would be necessary to isolate the organic compounds that are produced.[3] In order to reduce separations costs, it is possible that the phenolic pyrolysis products could be used as is, without any modifications. Also, it is possible that the pyrolysis process could be tailored to produce desired organic products. For example, Choi and Meier produced a lignin-derived bio-oil without catechols by using selective zeolite catalysts, which could open the possibility of producing thermoplastic resins from such bio-oils with little modification.[30] In this study, lignin-derived bio-oils produced through fast pyrolysis processes are investigated for their potential use as a chemical source in the development of bio-based VERs without the need for extensive separations.

Stanzione *et al*. investigated the use of lignin-derived bio-oils as a feedstock for thermosetting VERs by blending a bio-oil mimic based upon the composition of the bio-oil created by Jegers *et al*.[12, 33] This chapter presents an extension of the work done by Stanzione *et al*., whereby lignin-derived bio-oils were investigated as a source for VERs. In this work, multiple lignin-derived bio-oil mimics were made to easily prove whether such bio-oils can be used to produce high performance plastics. The composition of each lignin-derived bio-oil mimic was determined based on five lignin-derived bio-oil compositional studies.[26, 30-33] These studies were selected because fast pyrolysis

techniques were utilized and detailed compositional analyses of the lignin-derived bio-oil products were provided. Each bio-oil was mixed and converted into a VER through a one-step methacrylation reaction with methacryloyl chloride. The resins were analyzed by ^{1}H NMR spectroscopy, GPC, and FTIR. The thermomechanical properties of the functionalized bio-oil resins and plastics are reported and compared to both each other and a commercial VER equivalent.

3.2 Experimental

3.2.1 Materials. All chemicals were used as received. Guaiacol (≥99 %), catechol (≥99 %), 4-methylcatechol (98 %), *p*-cresol (≥99 %), vanillin (99 %), phenol (≥99 %) methacryloyl chloride (97 %, contains 200ppm monomethyl ether inhibitor), trimethylamine (99 %), dichloromethane (99.9 %, Optima™), tetrahydrofuran (99.9 %, ACS reagent grade), and hydrochloric acid (32 %) were purchased from Fisher Scientific. Sodium sulfate (≥99 %), 4-methylguaiacol (≥99 %), 4-ethylguaiacol (≥98 %), 4-propylguaiacol (≥98 %), and 4-vinylguaiacol (≥ 98%) were purchased from Sigma-Aldrich. Deuterated dimethyl sulfoxide (DMSO-d_6) was purchased from Acros Organics. Compressed argon was purchased from Praxair (99.998 %). A mixture of 50 % trivalent organic chromium complexes and 50 % phthlate esters, AMC-2, was purchased from AMPAC Fine Chemicals (Rancho Cordova, CA) and used as a catalyst in the methacrylation of diglycidyl ether of bisphenol A (Epon 828). Epon 828 was purchased from Momentive (see Section 4.2.2). Trigonox® 239, which contains 45 % cumene hydroperoxide, was purchased from AkzoNobel Polymer Chemicals and utilized as a free radical initiator.

3.2.2 Lignin-derived bio-oil compositions. Lignin-derived bio-oils are characterized by having a high percentage of phenolic compounds. Also, many of the same phenolic compounds appear in high concentrations across multiple sources. Three lignin-derived bio-oil mimics were made by blending the phenolics that appear most often in the organic phase of lignin pyrolysis products. *Figure 7* shows the phenolic compounds that were used to create the lignin-derived bio-oil mimics. Each chemical can be categorized into guaiacols, phenols, or catechols. Guaiacol type molecules include guaiacol, 4-methylguaiacol, 4-ethylguaiacol, 4-propylguaiacol, 4-vinylguaiacol, and vanillin. Phenol type molecules include *p*-cresol and phenol. Catechol type molecules include catechol and 4-methylcatechol.

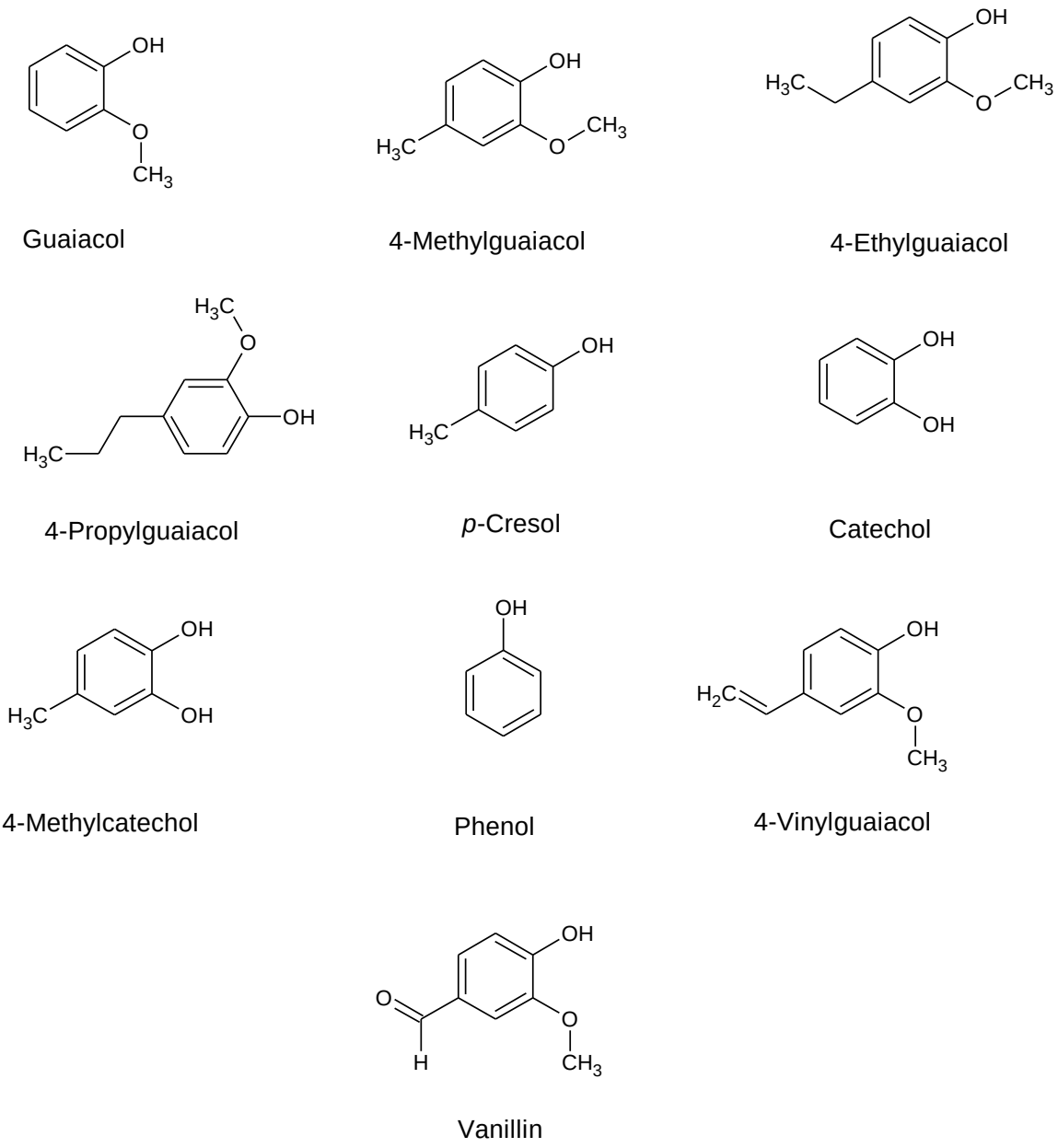

Figure 7. Phenolic chemicals that were utilized in creating the bio-oils presented in this thesis.

The composition of lignin-derived bio-oil mimic 1 (BO1) was determined using the data from Farag, Jessop, and Chaouki (2014)[26], Choi and Meier (2013)[30], Jegers and Klein (1985)[33], and Shen, Lou, Wang, and Fang (2010).[31] Lignin-derived bio-oil

mimic 2 (BO2) was created by incorporating data from an additional lignin-derived bio-oil study by Jiang, Nowakowski, and Bridgewater (2010).[32] These studies were selected because fast pyrolysis was utilized and detailed compositional analyses of the bio-oil products were provided. In addition, four of the five sources utilized lignin generated through the Kraft process and similar experimental conditions were used throughout.

Although many of the same chemicals appear in high concentrations across multiple sources, there are variations in the type and concentration of chemicals in the pyrolysis products. In BO1 and BO2, the concentration of each oil phase pyrolysis phenolic product was averaged across all sources and conditions within each source. Compounds not present in a pyrolysis product were excluded from the average. Also, the number of times each compound appeared across every source was counted and is referred to as the count. An objective function was used in order to equally weigh the average concentration and the count of each compound, which is shown in Equation 11.

$$Objective = \frac{AVG\ wt.\%}{Highest\ AVG\ wt.\%} + \frac{Count}{Highest\ Count} \tag{11}$$

The compounds with the highest objective number were utilized in BO1 and BO2. Table 3 shows the average weight percent and count of the chemicals with an objective greater than or equal to 1 for BO1. A similar table was made for BO2 and is shown in Table 4.

Table 3.

Average weight percent, count, and objective number for the single aromatic molecules used to generate BO1

Compound	Average wt. %	Count	Objective
Guaiacol	15.2	20	2.0
4-Methylguaiacol	10.7	19	1.7
Phenol	5.8	20	1.4
4-Methylcatechol	8.0	17	1.4
Catechol	7.9	16	1.3
4-Ethylguaiacol	5.5	18	1.3
4-Ethylcatechol	4.3	16	1.1
4-Methylphenol	3.6	17	1.1
2-Methylphenol	4.4	15	1.0
4-Propylguaiacol	4.2	15	1.0
4-Ethylphenol	3.1	16	1.0
Syringol	12.8	3	1.0

Table 4.

Average weight percent, count, and objective number for the single aromatic molecules used to generate BO2

Compound	Average wt. %	Count	Objective
4-Methylcatechol	8	17	0.9
Guaiacol	11.4	30	1.5
4-Vinylguaiacol	11.1	19	1.1
4-Methylguaiacol	10.7	19	1.1
4-Methylphenol	4.4	15	0.7
Catechol	6.5	25	1.1
4-Ethylguaiacol	5.5	18	0.8
Phenol	4.3	30	1.2
4-Propylguaiacol	4.2	15	0.7
4-Ethylphenol	2.7	19	0.7
o-Methylphenol	3.6	17	0.7
4-Ethylcatechol	4.3	16	0.7
5-hydroxyvanillin	24	4	1.1
Syringol	7.9	13	0.8

4-ethylcatechol, 2-methylphenol, and 4-ethylphenol were excluded in BO1 due to the similarity in structure to phenolics of higher concentration. Instead, the weight percent of these compounds were added to compounds of similar structure. The weight percent of 2-methylphenol and 4-ethylphenol were added to 4-methylphenol, and the weight percent of 4-ethylcatechol was added to 4-methylcatechol. Syringol was not included in BO1 due to its low count, despite having a relatively high average weight percent.

A similar procedure was used to create BO2, where the weight percents of 4-ethylphenol and *o*-methylphenol were added to 4-methylphenol, and the weight percent of 4-ethylcatechol was added to 4-methylcatechol. Syringol and 5-hydroxyvanillin were excluded from BO2 because of low counts, despite having relatively high average weight percents, especially 5-hydroxyvanillin. Due to the fact that the average wt. % across all sources in BO1 and BO2 did not add up to 100 %, the weight percents were scaled appropriately in order for BO1 and BO2 to sum to 100 %.

Lignin-derived bio-oil mimic 3 (BO3) was created based on Choi and Meier (2013), who used zeolite catalysts to produce a lignin-derived pyrolysis oil phase product without catechols.[30] Specifically, the catalysts were HZSM-5 (used in the pyrolysis processing of biomass[66-68]), FCC (commonly used in the refining of petroleum[69]), and Olivine (commonly used in tar cracking steam gasification processes[69]).[30] Levoglucosan, isoeugenol, acetoguaiacone, and 3-methylguaiacol were excluded from BO3 due to low concentrations and high costs. It is anticipated that due to their low concentrations, there would not be a significant effect on polymer properties. In addition, BO3 contains approximately 8 wt. % of acetic acid, which was not incorporated in BO3

and is anticipated to be easily separated industrially via techniques such as vacuum distillation.[12] The compositions of BO1, BO2, and BO3 are shown in Table 5. BO3 is characterized by the absence of catechols and the presence of 4-vinylguaiacol (the only crosslinking monomer).

Table 5.

Concentrations of all lignin-derived bio-oil mimics

Compound	**BO1 wt. %**	**BO2 wt. %**	**BO3 wt. %**
Guaiacol	21	15	55.5
4-Methylcatechol	17	16	0
4-Methylguaiacol	15	14	15.7
4-Methylphenol	15	14	0
Catechol	11	8	0
Phenol	8	6	2.0
4-Ethylguaiacol	7	7	8.2
4-Propylguaiacol	6	5	2.1
4-vinylguaiacol	0	15	10.5
Vanillin	0	0	6.0

3.2.3 Synthesis of MLMCs. The phenolics in BO1, BO2, and BO3 were blended and methacrylated as shown in *Figure 8*.

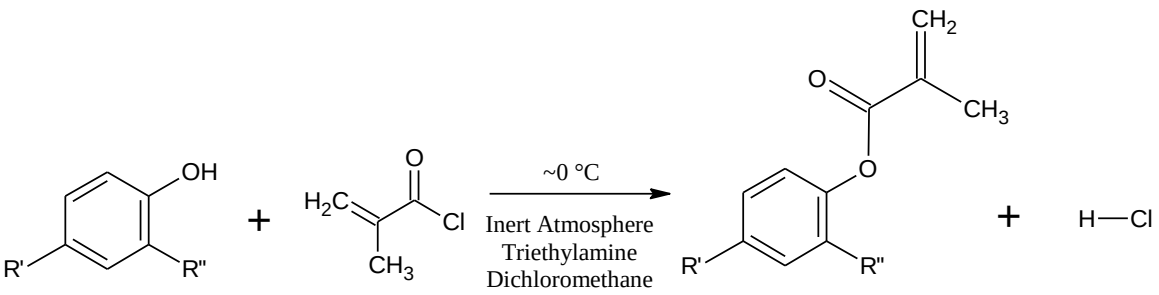

guaiacol: R’ = H, R’’ = -OCH_3
4-methylcatechol: R’ = -CH_3, R’’ = -OH
4-methylguaiacol: R’ = -CH_3, R’’ = -OCH_3
4-methylphenol: R’ = -CH_3, R’’ = H
catechol: R’ = H, R’’ = -OH
phenol: R’ = R’’ = H
4-ethylguaiacol R’ = -CH_2CH_3, R’’ = -OCH_3
4-propylguaiacol R’ = -$CH_2CH_2CH_3$, R’’ = -OCH_3
4-vinylguaiacol R’ = -OCH_3, R’’ = -CH_2CH_2
vanillin: R’ = -COH, R’’ = OCH_3

1: R’ = H, R’’ = -OCH_3
2: R’ = -CH_3, R’’ = -$OCOCCH_2CH_3$
3: R’ = -CH_3, R’’ = -OCH_3
4: R’ = -CH_3, R’’ = H
5: R’ = H, R’’ = -$OCOCCH_2CH_3$
6: R’ = R’’ = H
7: R’ = -CH_2CH_3, R’’ = -OCH_3
8: R’ = -$CH_2CH_2CH_3$, R’’ = -OCH_3
9: R’ = -OCH_3, R’’ = -CH_2CH_2
10: R’ = COH, R’’ = OCH_3

Figure 8. Esterification reaction used to methacrylate lignin-derived bio-oil mimics.

Methacryloyl chloride is highly reactive and does not require a catalyst.[70, 71] This reactant was utilized to methacrylate lignin-derived bio-oils due to the highly reactive, irreversible, nature of acid chloride reactions. In addition, this reaction does not require heating and proceeds rapidly at room temperature. All other common methacrylation reactants, which include methacrylic anhydride, methacrylic acid, and methyl methacrylate, are not as reactive and require a catalyst with heating.[57, 59, 72] In the work done by Stanzione *et al*., unreacted phenolic, unreacted methacrylic anhydride, methacrylic acid, and methacrylated topanol A are reported in the product after aqueous wash purifications (methacrylic anhydride was utilized for methacrylation).[7, 12] In

order to avoid the complications associated with the impurities in the work done by Stnazione *et al.*, methacryloyl chloride was chosen.

To 500 mL round bottom flasks, 25 g of each lignin-derived bio-oil mimic was dissolved in 60 mL of methylene chloride with a stoichiometric amount of trimethylamine. Each reaction flask was placed in an ice bath. A 1.05 molar excess of methacryloyl chloride was dissolved in methylene chloride (1:1 weight ratio) and added drop wise to the dissolved bio-oil under an argon atmosphere. The mixture was subject to vigorous mixing throughout the dropping process. As methacryloyl chloride reacts with the phenolics, hydrochloric acid is formed, which forms a trimethylamine-HCl salt precipitate.

Subsequent washes with sodium hydroxide (2.5M) and hydrochloric acid (1M) were performed before drying over sodium sulfate and concentrating under reduced pressure. A methacrylated bio-oil is referred to as MBO, where MBO1, MBO2 and MBO3 represent the methacrylated versions of BO1, BO2, and BO3, respectively.

MBO1, MBO2, and MBO3 were characterized by means of ^{1}H NMR (400.13 MHz, 16 scans at 298.2K) using a Varian Mercury 400 MHz Nuclear Magnetic Resonance System. The ^{1}H NMR of each individual methacrylated compound was compared to the ^{1}H NMR of each MBO. FTIR spectroscopy characterization was performed on a Nicolet 6700 FTIR. In the mid-IR range, 32 cumulative scans were taken at a resolution of 2 cm^{-1}. Also, gel permeation chromatography (GPC) was performed using a Waters 2695 GPC fitted with Waters Styragel HR4, HR2, and HR1 columns in series using Optima™ THF (1 mL min^{-1}) as the mobile phase. A Waters 2414 Refractive Index Detector was used and GPC samples were prepared in a concentration of 2 mg/mL.

3.2.4 Resin curing. Each MBO was free radically polymerized using Trigonox® 239 (1.5 wt % of total resin mass) as a free radical initiator.[13, 73, 74] The resins were degassed until no visible bubbles remained, transferred into a silicone rubber mold, and purged with argon for 20 minutes. All MBOs were cured at 90 °C for 4 hours with a subsequent post cure at 160 °C for 2 hours. The plastics were allowed to cool overnight to room temperature before removal from the vacuum oven.

3.2.5 Extent of cure. Near-infrared (near-IR) spectra of the uncured and cured MBO resins were obtained using a Nicolet iS50 FT-IR in order to determine the extent of cure of the plastics. Near-IR spectra were taken in the 4000-7000 cm^{-1} range with 32 cumulative scans at a 2 cm^{-1} resolution. The cured plastics (typically of 3-4 mm thickness) were cleaned with acetone and dried thoroughly before the near-IR spectra was taken. The MBO resins were placed in a glass vessel with a thickness of 3 mm when obtaining the near-IR spectra. The extent of cure was measured by calculating the percent decrease of the methacrylate bond (6165 cm^{-1}) after curing.[12] The phenol group peak (4623 cm^{-1}) was used as an internal standard because it is not affected by the cure. Equation 12 was used to calculate the extent of cure for each MBO resin. $ABS_{wavelength}$ refers to the peak height at the subscripted wavelength.

$$X = \frac{\left(\frac{ABS_{6165cm^{-1}}}{ABS_{4263cm^{-1}}}\right)_{unreacted} - \left(\frac{ABS_{6165cm^{-1}}}{ABS_{4263cm^{-1}}}\right)_{reacted}}{\left(\frac{ABS_{6165cm^{-1}}}{ABS_{4263cm^{-1}}}\right)_{unreacted}} \quad (12)$$

3.2.6 Polymer properties. Dynamic mechanical analysis (DMA) was used to determine the thermo-mechanical properties of each thermoset, which includes the glass transition temperature (T_g), storage modulus (E') at 25 °C, rubbery temperature, rubbery

E', and effective molecular weight between crosslinks (M_c). M_c was calculated using Equation 16,

$$M_c = \frac{3RT\rho}{E} \tag{16}$$

where R is the ideal gas constant, T is absolute temperature, and ρ is the sample density at room temperature. The rubbery E' and T were defined as the point at which the storage modulus increases with increasing temperature, in the rubbery region.[75] The density of the polymer was determined using Archimedes' principle at room temperature.[76] Typical DMA sample dimensions were 35 x 12 x 3 mm^3 and a single cantilever geometry was used. The temperature was increased from 0 to 250 °C at a rate of 2 °C per minute, while oscillating at 1 Hz with a 7.5 μm deflection. A Poissons ratio of 0.35 was used.

3.3 Results and Discussion

3.3.1 Resin characterization. After aqueous washing purification, MBO1 and MBO2 are transparent liquids with a yellow hue, while MBO3 is a clear, colorless liquid. The ^{1}H NMR spectra for MBO1, MBO2, and MBO3 are shown in *Figure 9*, *Figure 10*, and *Figure 11*, respectively. The numbers on each peak correspond to the methacrylated compound numbers that are shown in *Figure 8*.

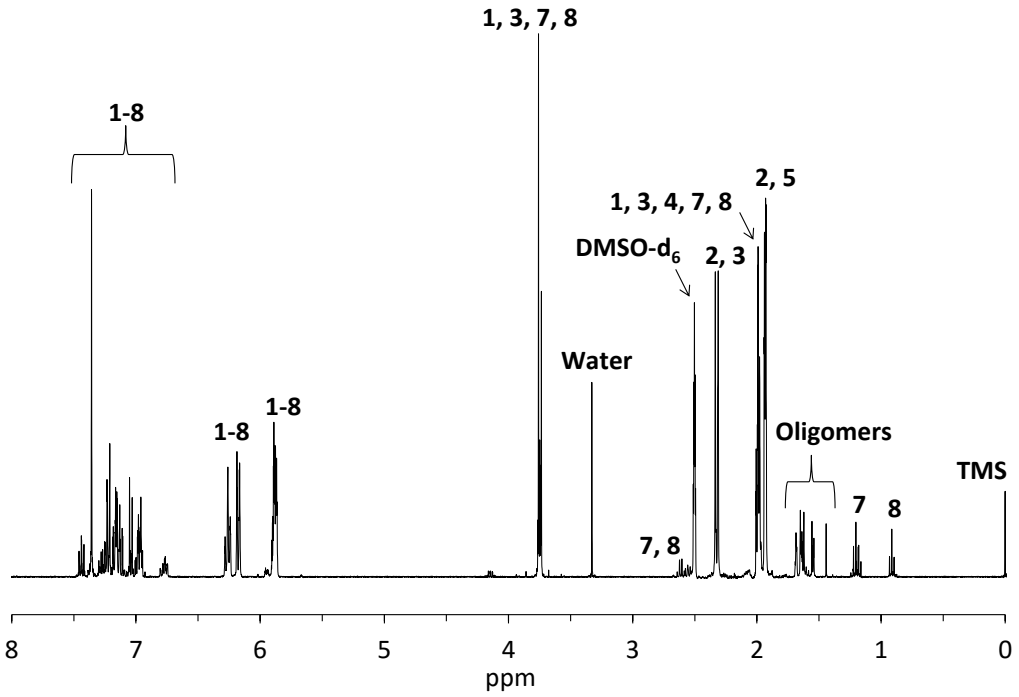

Figure 9. ^{1}H NMR spectra of MBO1 after aqueous washing. The peak labels correspond to the methacrylated compound numbers in *Figure 8*.

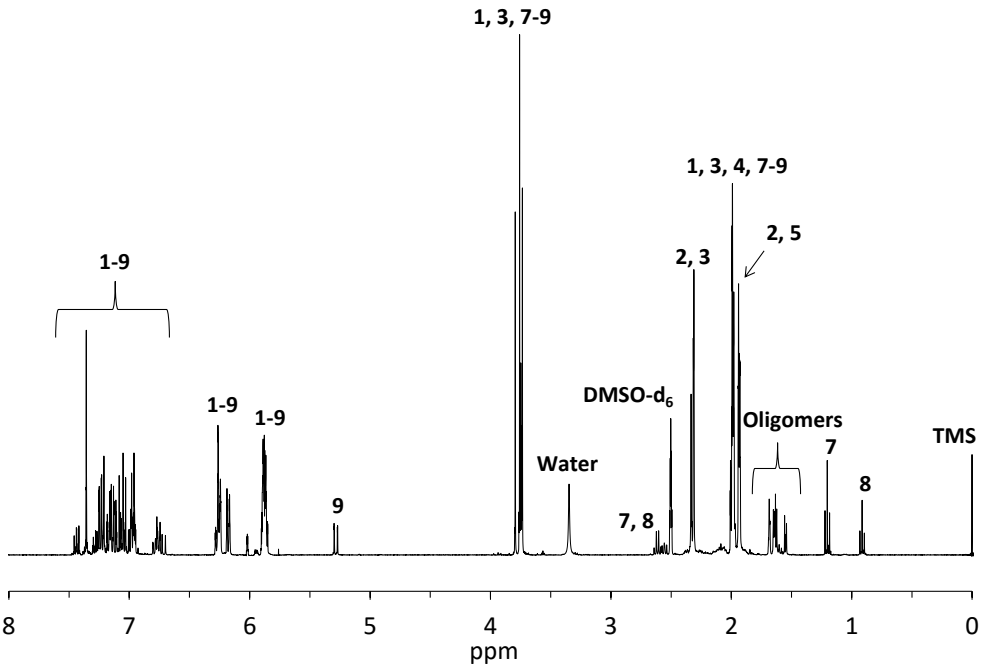

Figure 10. ^{1}H NMR spectra of MBO2 after aqueous washing. The peak labels correspond to the methacrylated compound numbers in *Figure 8*.

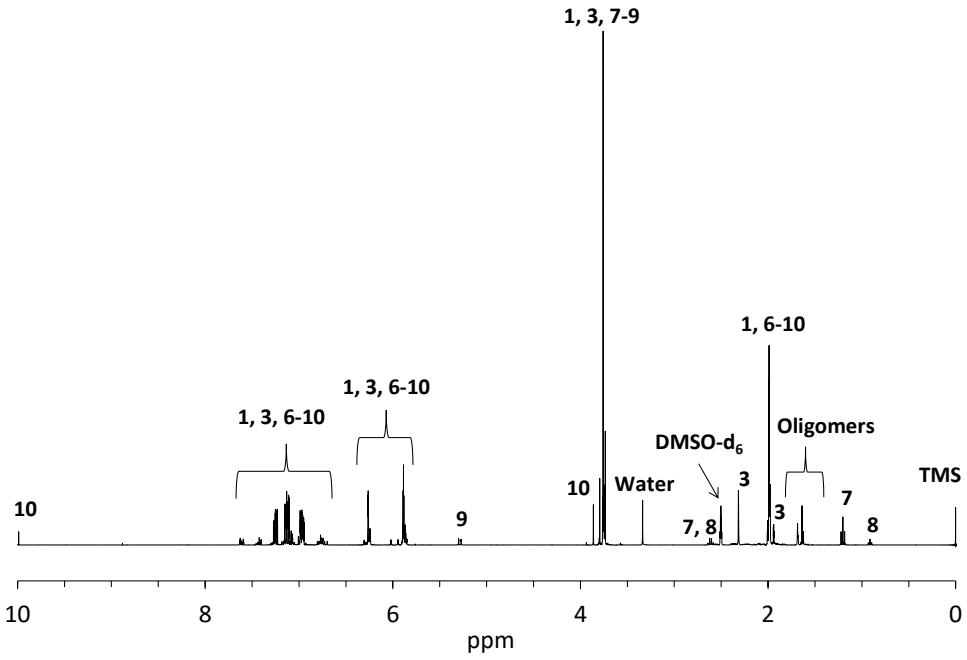

Figure 11. ^{1}H NMR spectra of MBO3 after aqueous washing. The peak labels correspond to the methacrylated compound numbers in *Figure 8*.

The methacrylation reaction utilizes excess methacryloyl chloride and triethylamine in dichloromethane. Unreacted phenolics, methacryloyl chloride, and triethylamine-HCl salts are removed through aqueous washing, which was confirmed via ^{1}H NMR analysis. Excess triethylamine and dichloromethane are evaporated off during the drying procedure. Based on the ^{1}H NMR spectra of each methacrylated phenolic present in MBO1, MBO2, and MBO3, all peaks are accounted for in *Figure 9*, *Figure 10*, and *Figure 11*, except the peaks labeled "oligomers". When compared to the methacrylic anhydride methacrylation route, the resulting MBO resin does not contain unreacted phenolics, methacrylic anhydride, methacrylic acid, or methacrylated inhibitors

present.[12] These impurities in methacrylated bio-oils synthesized via methacrylic anhydride have been reported to sum to approximately 14 mol %.[12]

The oligomers are hypothesized to form during the methacryloyl chloride methacrylation reaction due to small pockets of heat that spark the auto-polymerization of all methacrylates present. The auto-polymerization is thought to be readily terminated as the small pocket cools back to the bulk reaction temperature (ice bath conditions) and the radical is suppressed. In a study by Rojo *et al*., oligomers were formed when methacrylating eugenol with methacryloyl chloride under similar reaction conditions.[77]

In order to determine the approximate molecular weight of MBO1, MBO2, and MBO3, GPC was performed. *Figure 12* shows the GPC trace for MBO1, MBO2, MBO3, and polystyrene standards.

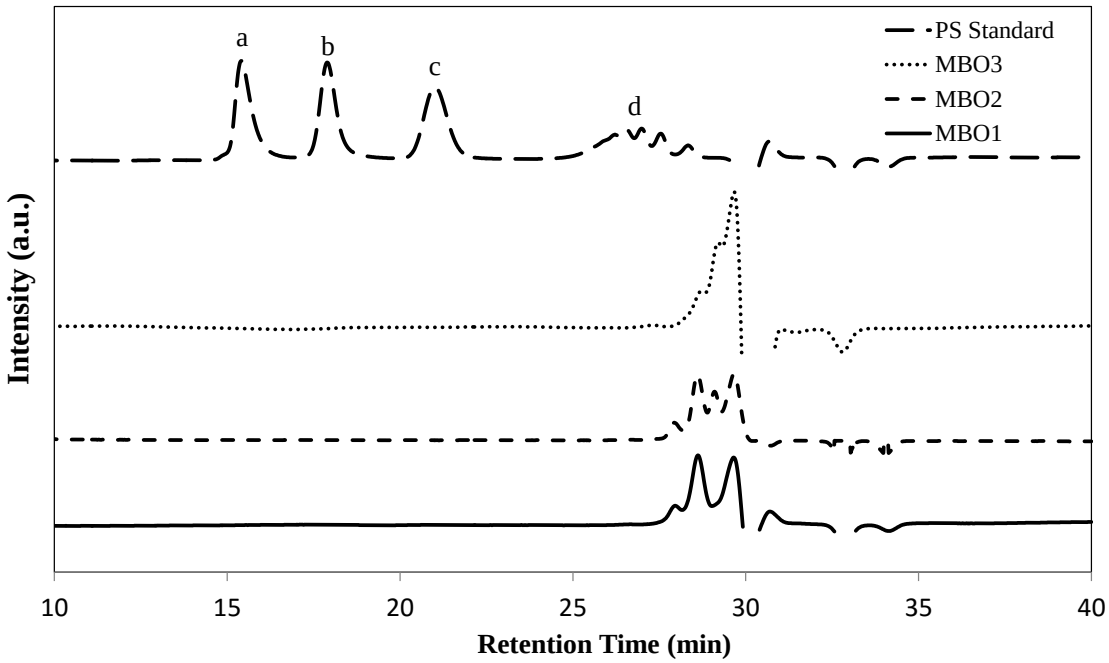

Figure 12. GPC trace for MBO1, MBO2, MBO3, and polystyrene standards. The number average molecular weights for the polystyrene (PS) standard are: a - 532,000 Da, b - 59,300 Da, c - 8,650 Da, and d - 492 Da.

For MBO1, MBO2, and MBO3, the GPC traces show that the molecular weights are less than 400 g/mol when compared to polystyrene standards. The GPC column was not able to provide adequate separation in order to determine exact molecular weights, but approximations can still be made. The predicted retention time of methacrylated 4-methylcatechol (M-4MC) was compared to the GPC traces of MBO1, MBO2, and MBO3 (*Figure 13*). The predicted retention time of M-4MC was determined using a standard curve generated from pure methacrylated phenol (MP), methacrylated guaiacol (MG), and methacrylated 4-propylguaiacol (M4PG, see Chapter 4 for synthesis) GPC traces. The standard curve can be found in Appendix C (*Figure 36*).

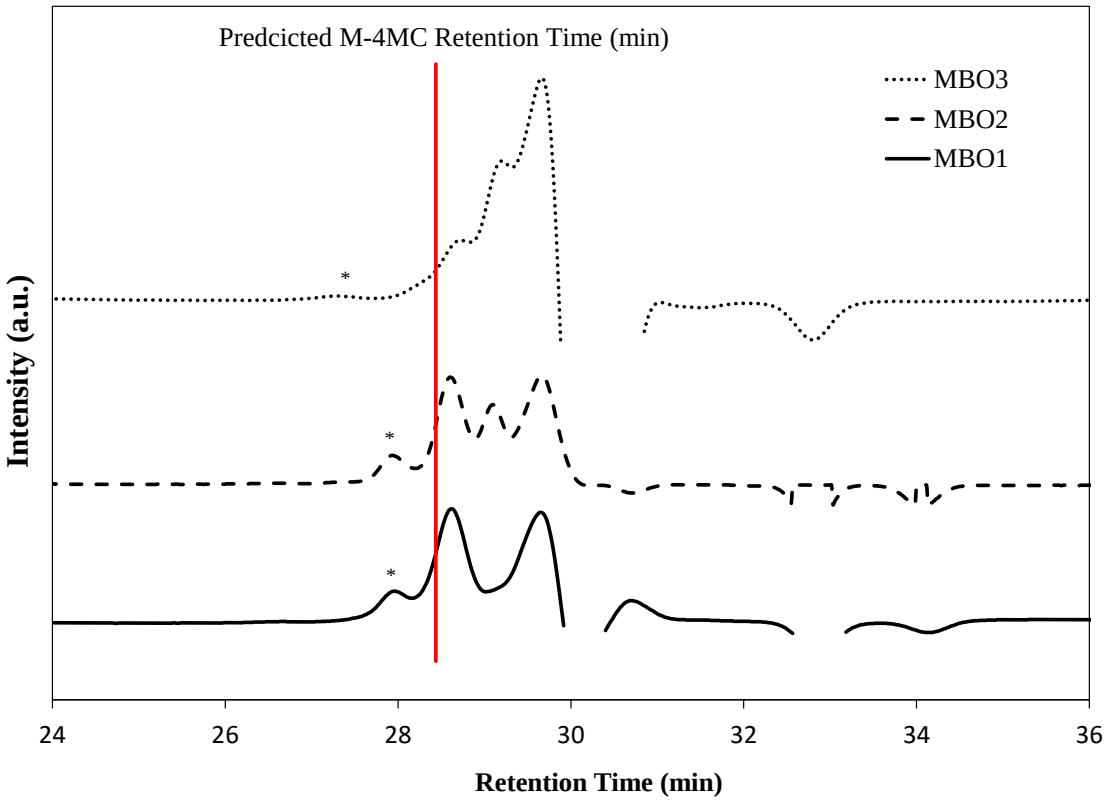

Figure 13. The GPC traces of MBO1, MBO2, and MBO3 are shown. The predicted retention time of methacrylated 4-methylcatechol (the highest MW methacrylated lignin model compound) is given by the vertical line at a retention time of 28.3 minutes. The peaks represented by * are hypothesized to be "oligomers".

The small peaks, represented by *, on the MBO1, MBO2, and MBO3 traces are hypothesized to signify "oligomers". The predicted M-4MC retention time is hypothesized to not be at the local minimum after the oligomer (*) peak due to error within the standard curve. The R^2 value for the standard curve was found to be 0.8627 and was generated with three data points. In addition, the GPC columns utilized are designed for high molecular weight polymers and not single aromatic monomers. Overall, the GPC data shows that there are no high molecular weight polymer chains

present in MBO1, MBO2, and MBO3. In order characterize the “oligomers”, future experimentation involving TLC, flash chromatography, HPLC, and subsequent proton and carbon NMR of isolated “oligomers” are recommended.

3.3.2 Extent of cure. Photos of MBO1, MBO2, and MBO3 are shown in *Figure 14*.

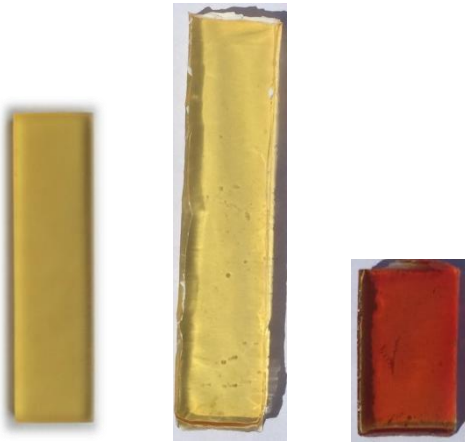

Figure 14. Photos of cured (a) MBO1, (b) MBO2, and (c) MBO3.

When polymerized, MBO1, MBO2, and MBO3 are hard, transparent plastics. MBO1 and MBO2 have a yellow hue, similar to that of their respective resins; however, MBO3 has an orange hue that is in contrast to its colorless resin. The yellowish hues are due to Trigonox 239, which was used as an initiator in the polymerization reactions. The near-IR spectrum of each MBO resin and cured MBO resin was obtained and are shown in *Figure 15*.

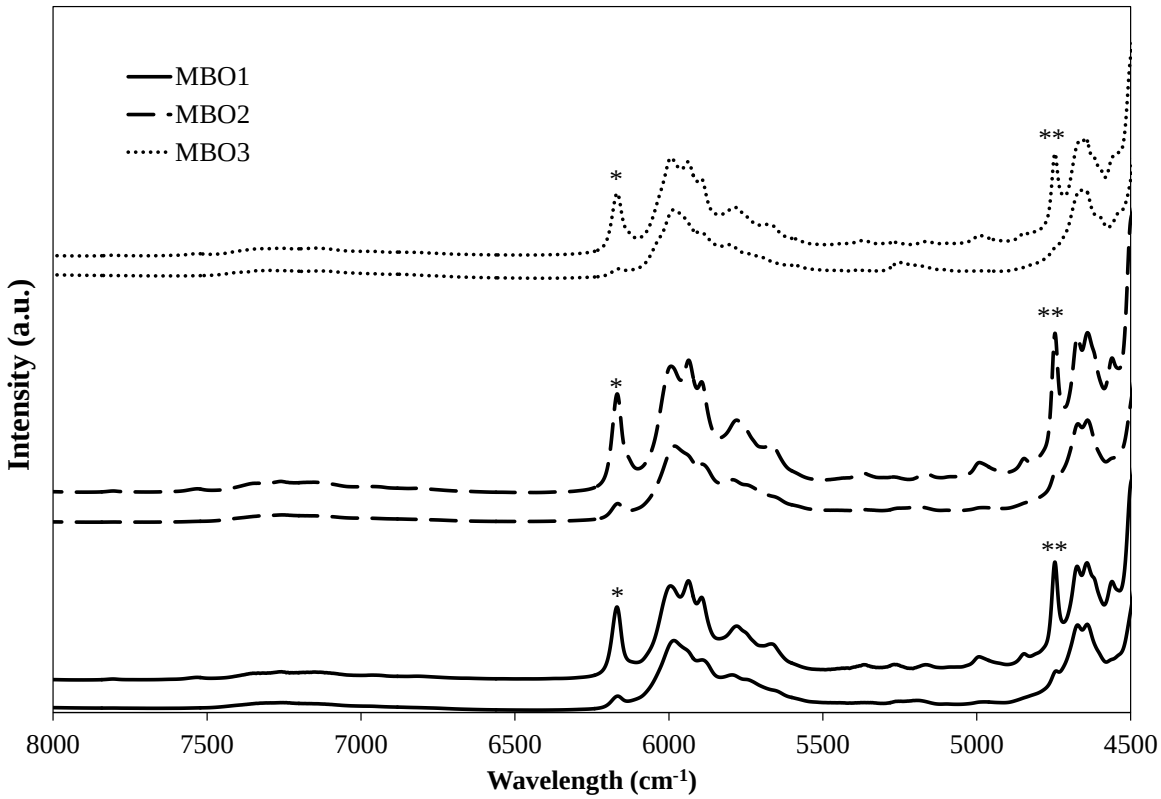

Figure 15. Near-IR extent of cure for MBO1, MBO2, and MBO3. The methacrylate C=C bond peaks are labeled * and the $=CH_2$ peaks are labeled **.

The peaks at 6165 cm^{-1} and 4623 cm^{-1} represent the methacrylate (=C-H) and phenyl groups, respectively. The methacrylate (=C-H) group also absorbs at 4743 cm^{-1}, but extent of cure measurements are not precise using this band due to the sharp baseline drop at nearby wavelengths. During the free radical polymerization, the methacrylate (=C-H) bond reacts to form a carbon-carbon single bond (-C-C) bond, which results in the decreased peak height that is observed at 6165 cm^{-1} and 4743 cm^{-1}. The calculated extent of cure (Equation 12) for each MBO can be found in Table 6.

Table 6.

Extent of Cure for MBO1, MBO2, and MBO3

System	Extent of Cure (%)
MBO1	89.5 ± 0.8
MBO2	88.0 ± 1.6
MBO3	94.7 ± 1.2

The extents of cures are similar to what was reported by Stanzione et al, whom reported an extent of cure of 92.9 % ± 0.8 for their MBO.[12] MBO2 has a slightly lower extent of cure at 88.0 %, while MBO3 has a slightly higher extent of cure at 94.7 %. It is possible the discrepancy between each MBO, including the MBO reported in Stanzione et al, is related to the amount of crosslinking monomers present. MBO 2 has the highest percent of crosslinking monomers at 38 mol % and has the lowest extent of cure. MBO1 has a lower percent of crosslinking monomers at 29 mol % and has a higher extent of cure than MBO2. This trend continues for MBO3 and is also consistent based on the bio-oil from Stanzione et al.[12] With a higher concentration of crosslinking monomers, the curing resin becomes diffusion limited quicker into the cure, and therefore the extent of cure is reduced.[78] Although there is a slight discrepancy in the extent of cure of each MBO cured resin, all are considered high, which ensures robust polymer properties that are minimally affected by low extent of cures. In the future, cure kinetics will be studied in order to confirm the extent of cure obtained via near-IR.

3.3.3 Polymer properties. DMA was used to determine the thermo-mechanical properties of MBO1, MBO2, and MBO3, which includes glass transition temperatures (T_g*s*), storage moduli (*E's*) at 25 °C, rubbery temperatures, rubbery *E's*, and the effective molecular weights between crosslinks (M_c*s*). The storage and loss moduli of MBO1,

MBO2, and MBO3, are plotted as a function of temperature in *Figure 16*. Table 7 shows the thermo-mechanical properties for MBO1, MBO2, and MBO3. The storage modulus is a measure of stored energy and the loss modulus represents the heat lost during a loading cycle.[65] Tan δ is defined as the ratio of the loss modulus to the storage modulus and represents the damping factor or loss tangent.[65]

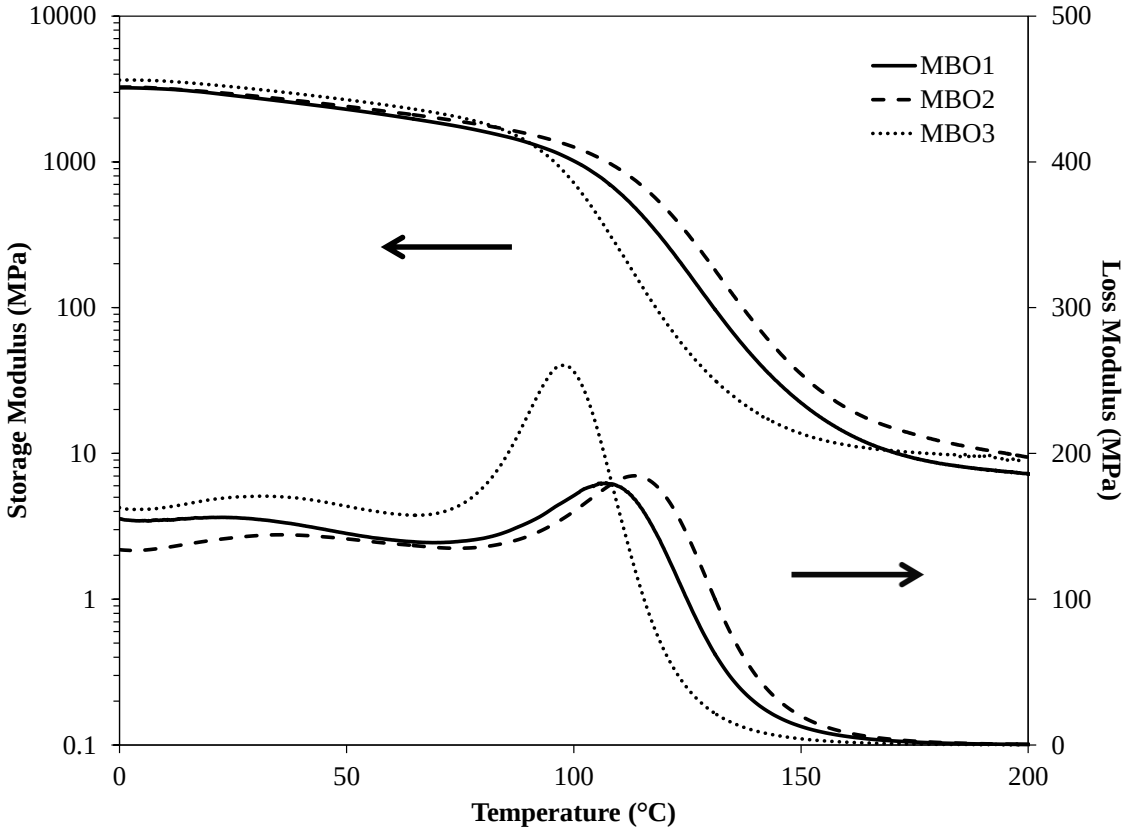

Figure 16. DMA results for MBO1, MBO2, and MBO3.

Table 7.

Thermo-mechanical properties of MBO1, MBO2, and MBO3

System	***E′* at 25 (GPa)**	***E′(T)* Inflection (°C)**	**Peak of *E″* (°C)**	**Peak of tan *δ* (°C)**	**Rubbery *E′* (MPa)**	**rubbery *T* (°C)**	***ρ* at 25 °C (g cm^{-3})**	**eff. *Mc* (g mol^{-1})**
MBO 1	3.0 ± 0.2	124.2 ± 2.2	126.7 ± 3.0	151.8 ± 4.2	12.1 ± 3.2	201.8 ± 4.2	1.2 ± 0.00	1270 ± 303
MBO2	3.3 ± 0.1	129.8 ± 1.2	128.8 ± 0.6	157.4 ± 0.6	40.7 ± 4.2	207.4 ±0.6	1.2 ± 0.00	356 ± 35
MBO 3	3.6 ± 0.1	98.6 ± 0.5	100.4 ± 0.6	122.04 ± 0.6	9.8 ± 0.6	172.0 ± 0.6	1.3 ± 0.04	1463 ± 107
Stanzione *et al.* MBO [12]	3.2 ± 0.3	116 ± 1.7	115 ± 0.3	140 ± 0.1	5.0 ± 0.4	200 ± 23	1.219 ± 0.00	2882 ± 11

The *E′*s of MBO1, MBO2, and MBO3 at 25 °C are 3.0 ± 0.2 GPa, 3.3 ± 0.1 GPa, and 3.6 ± 0.1 GPa, respectively. The storage modulus reported by Stanzione et al. was 3.2 ± 0.3 GPa.[12] Generally, as the concentration of methoxy substituents increases, the storage modulus increases. MBO3 has the highest storage modulus where 97 mol % of the methacrylated phenolics have a methoxy group, while 44 mol % of the methacrylated phenolics in MBO1 have a methoxy group. In MBO2 and the MBO reported by Stanzione *et al.*, 50 mol % and 72 mol % of the methacrylated phenolics have methoxy groups, respectively. The MBO reported by Stanzione *et al.* does not follow the trend in this study; however, it contains unreacted phenolics, methacrylic anhydride, methacrylic acid, and methacrylated topanol A that may have an effect on the storage modulus.[7, 78] When compared to a commercial VER, 1:1 VE828:St (see Chapter 4), the storage modulus of each MBO is higher due to the presence of the methoxy groups. The heightened *E′* at 25 °C is a result of enhanced hydrogen bonding due to the methoxy group.[79]

The loss modulus curves of MBO1, MBO2, and MBO3, as well as the MBO reported by Stanzione *et al.*, display beta relaxations between 15-70 °C. This relaxation is caused by the gradual diminishment of hydrogen bonding and van der Waals attractions, which releases heat and, therefore, appears as a slight peak in loss modulus curves.[80] Hydrogen bonding is enhanced by the methoxy group that is present on guaiacol, 4-methylguaiacol, 4-ethylguaiacol, 4-propylguaiacol, and 4-vinylguaiacol.[72]

Using the theory of rubber elasticity, the effective molecular weights between crosslinks were determined.[75] The rubbery modulus was defined as the *E′* at the local minimum within the rubbery region, which was between 171 °C and 203 °C for MBO1,

MBO2, and MBO3. The M_c values for MBO1, MBO2, and MBO3 were 1270 ± 303, 356 ± 35, and 1463 ± 107 g/mol, respectively. It is expected that the M_cs would decrease with an increasing concentration of crosslinking monomers. The M_c data for the cured MBO resins follow this trend; however, it is expected that MBO1 and MBO3 would have a larger difference between M_c values due to the difference in crosslinking monomers Within experimental error, there is not a clear difference in M_c values when comparing MBO1 and MBO3, although there is a 20 mol % difference in crosslinking monomers. The theory of rubber elasticity assumes that the plastic is lightly crosslinked, there are no intramolecular cyclizations, and all functional groups are equally reactive.[75] The similarity in the M_c*s* could be due to intermolecular cyclization occurring in MBO1 and not in MBO3. MBO1 has a higher concentration of di-functional molecules that have functional groups *ortho* to each other, which is hypothesized to increase the probability of intramolecular cyclization. This hypothesis is supported by experiments presented in Stanzione's Ph.D. thesis.[72] Intramolecular cyclization causes the di-functional molecule to act as a chain extender instead of a crosslinking agent, which can be seen in *Figure 17* (adapted from Ohya *et al.*).[81]

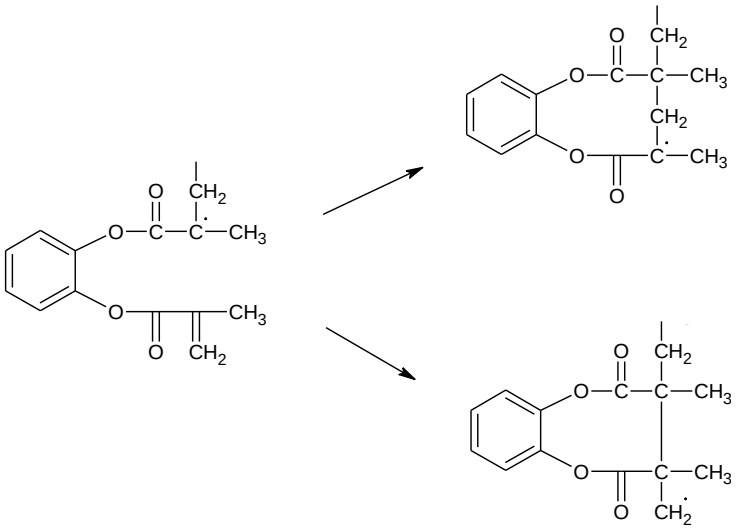

Figure 17. Intramolecular cyclization of methacrylated catechol, adapted from Ohya *et al.*[81]

An increase in intramolecular cyclization would increase the molecular weight between crosslinks. Also, MBO2 and MBO3 contain 4-vinylguaiacol, which has a styrenic vinyl group that is known to have a curing reactivity that is higher than methacrylate vinyl ester groups.[82, 83] Future experiments are recommended in order to quantify the styrenic vinyl reactivity using FTIR spectroscopy in MBO2 and MBO3. Intermolecular cyclization also affects the polymer network by adding a bulky side group, the double ring structures that are formed, which physically and thermodynamically force greater separation between polymer chains.

In this study, T_g was based on the peak of the E'' curve, which is quantitatively similar to the inflection of the E' curve. The T_g is often predicted by the peak of the tan δ curve; however, the tan δ T_g is normally higher than that of the E'' and E' curve. Therefore, the peak of the E'' curve was used as a conservative value. The T_g data for

MBO1, MBO2, and MBO3 show that as the concentration of crosslinking monomers increases, the T_g increases. However, it is expected that a 9 mol % increase in crosslinking monomers between MBO1 to MBO2 would raise the T_g of the plastic by more than approximately 5 °C. To explain this, it is possible that the styrene vinyl on 4-vinylguaiacol has a marginal effect on the extent of crosslinking within the plastic; however, the low M_c for MBO2 implies that there is a significant increase in the amount of crosslinking when compared to MBO1. Also, intermolecular cyclization could be occurring; however, MBO1 has a slightly higher concentration of catechol and 4-methylcatechol.

Another explanation for the slight increase in T_g from MOB1 to MBO2 is through the presence of oligomers. Through ^{1}H NMR analysis, it can be seen that each MBO has oligomers. It was not possible to definitively quantify the extent at which oligomerization occurred in each bio-oil; however, it is possible that MBO2 has a greater concentration of oligomers than MBO1 (see *Figure 9* and *Figure 10*). Oligomers within the MBO resin are expected to act as plasticizers and therefore decrease the T_g of the cured plastic, assuming the reactive functionalities are less than two. If MBO2 has a higher concentration of oligomers than MBO1, the resulting T_gs would be closer in magnitude that what would be expected. Overall, the T_gs of MBO1 and MBO2 are comparable to that of a commercial VER, 1:1 VE828:St, which has a T_g of approximately 134 °C (see Chapter 4).

The heterogeneity of a polymer can be qualitatively determined through the broadness of the tan δ thermogram. In addition, a broad tan δ thermogram implies that the polymer exhibits a broader glass transition region.[84] For all MBO polymers, the width

of the tan δ peaks remains relatively constant, as shown in *Figure 18*. For the MBO polymers, as the number of crosslinking agents within the polymer is increased, the tan δ peak height decreases. This suggests that increasing the number of crosslinking agents within the MBO resin increases elastic behavior in the resulting plastic. This trend was observed in a study by Scott *et al*. with a bisphenol-A diglycidyl ether dimethacrylate : styrene blend.[78]

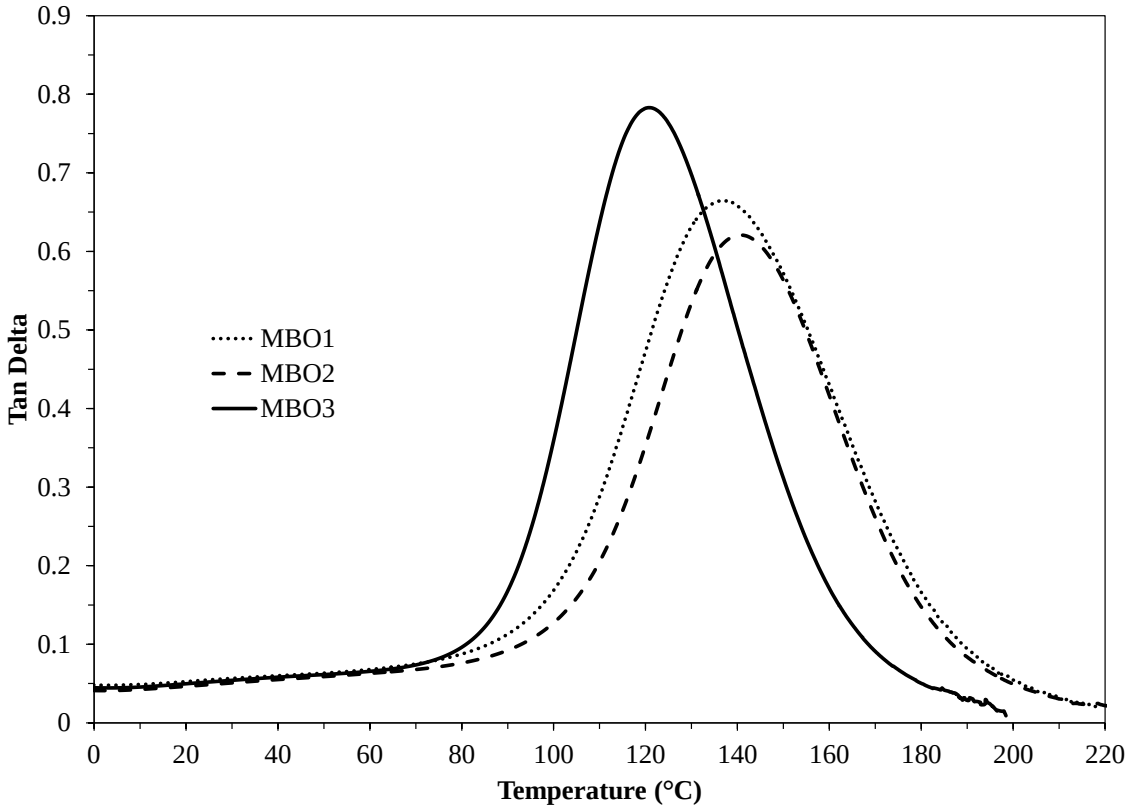

Figure 18. Tan δ results for MBO1, MBO2, and MBO3 as a function of temperature.

3.4 Conclusions

In this work, three lignin-derived bio-oil mimics, which include guaiacols, catechols, and phenols, were generated using five literature sources.[26, 30-33] All sources utilized a fast pyrolysis process and four of the five sources started with a Kraft lignin feedstock, with the other using an Organosolv lignin feedstock. In order to generate a representative lignin-derived bio-oil concentration based upon multiple studies, the average concentration across all sources and the number of instances a phenolic appeared were equally weighed and taken into account. The first bio-oil utilized four of the five sources, the second utilized all five sources, and the third was based on Choi *et al.* Each bio-oil was methacrylated using methacryloyl chloride via an esterification reaction. Due to the qualitative low viscosity of each MBO, it may be suitable for use as a reactive diluent in vinyl ester resins. Curing the resin resulted in hard, transparent plastics that had properties that are similar to that of their commercial counterparts. Also, various structure property relationships have been observed. As the concentration of methoxy groups increased, the storage modulus of the cured BO resin increased. Also, as the concentration of crosslinking monomers increased, the T_g increased. With increased research focus on the development and composition of lignin-derived bio-oils, this study has shown that it is possible to make viable vinyl ester thermosetting resins without the need to separate individual phenolic compounds. Also, this study has shown the variation in vinyl ester thermosetting plastic properties across multiple bio-oils of different phenolic concentrations.

Chapter 4

Methacrylated Lignin Model Compounds for use as Reactive Diluents in Vinyl Ester Resins

4.1 Introduction

In this study, three lignin model compounds (LMCs), phenol, guaiacol, and 4-propylguaiacol, were methacrylated and blended with a standard equivalent of a commercial vinyl ester resin (bismethacryl glycidyl ether of bisphenol A epoxy, VE828). These phenolic molecules were chosen because of their relatively high abundance in lignin-derived bio-oils (refer to Chapter 3), as well as their representative chemical structures.[26, 30, 31] Guaiacol and 4-propylguaiacol are guaiacol type molecules; where the difference between the two is that 4-propylguaiacol contains a propyl group *para* to the hydroxyl group. Phenol is a coumaryl-type molecule and does not have carbon chain substituents. Syringryl type molecules were not investigated due to their low reactivity and high expense; however, syringol is recommended in future studies to compliment this study.[72] Choosing phenol, guaiacol, and 4-propylguaiacol as the LMCs will provide insight into the effect of the methoxy group and the propyl group on the efficacy for these molecules to act as RDs in VERs.

The LMCs selected for this study were methacrylated utilizing an esterification reaction and purified through aqueous washes and subsequent column chromatography. Pure (≥97.5 mol %) methacrylated lignin model compounds (MLMCs) were blended with VE828 in a 1:1 weight ratio and bulk free radically polymerized to produce hard thermosets. The reactive diluent synthesis methods, as well as the extent of cure and vinyl ester polymer properties, are reported. In addition, styrene was utilized as a reactive diluent in a commercial VE828 resin for comparative purposes.

4.2 Experimental

4.2.1 Materials. Phenol (≥99 %), guaiacol (≥99 %), dichloromethane (99.9 %, Optima™), hexanes (99.9 %, certified ACS), ethyl acetate (99.9 %, certified ACS), styrene (inhibited with 10-15 ppm 4-*tert*-butylcatechol), and hydrochloric acid (32 %) were purchased from Fisher Scientific. Sodium sulfate (≥99 %), 4-propylguaiacol (≥98 %), methacrylic anhydride (94 %, contains 2000 ppm Topanol A inhibitor), and 4-dimethylaminopyridine (DMAP, 99 %) were purchased from Sigma-Aldrich. Deuterated dimethyl sulfoxide (DMSO-d_6) and deuterated chloroform ($CDCl_3$) were purchased from Acros Organics. Compressed argon was purchased from Praxair (99.998 %). A mixture of 50 % trivalent organic chromium complexes and 50 % phthlate esters, AMC-2, was purchased from AMPAC Fine Chemicals (Rancho Cordova, CA) and used as a catalyst in the methacrylation of diglycidyl ether of bisphenol A (Epon 828). Epon 828 was purchased from Momentive. Trigonox® 239, which contains 45 % cumene hydroperoxide, was purchased from AkzoNobel Polymer Chemicals and utilized as a free radical initiator.

4.2.2 Synthesis of vinyl ester resin. Bismethacryl glycidyl ether of bisphenol A epoxy (VE828) was synthesized through the reaction of diglycidyl ether of bisphenol-A (DGEBA/EPON828) and methacrylic acid, as shown in *Figure 19*.

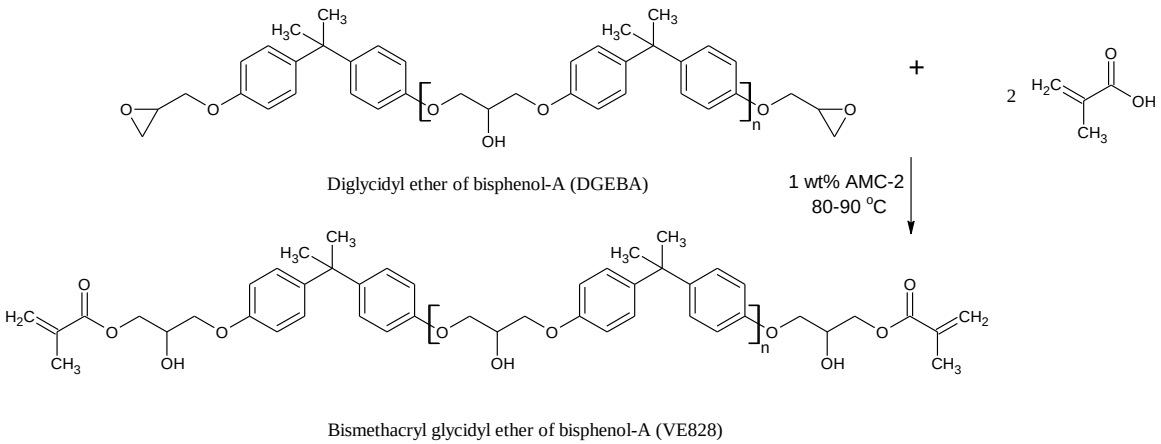

Figure 19. Synthesis of VE828 from DGEBA and methacrylic acid in the presence of AMC-2 catalyst at 80-90 °C, adapted from La Scala *et al.*[22]

The epoxy equivalent weight (EEQ) was 190 g/Eq and was determined using ASTM D1652. The molecular weight of Epon 828 is 340 + 284n, with n calculated to be 0.14. Approximately 500 g of Epon 828 was poured into a 1000 mL three necked round bottom flask. Methacrylic acid was added in the amount of 1.01 times the stoichiometric value and AMC-2 was added in the amount of 1.0 wt. % of the DGEBA. Using a mechanical mixer, the reaction solution was mixed at room temperature until homogeneous and subsequently heated to 70 °C. After the onset of an exotherm, the reaction mixture was kept at approximately 90 °C. In order to monitor the reaction, an ASTM acid number titration, as described in La Scala *et al.*, was utilized.[18, 22] The reaction was allowed to progress until the acid number was below 10.[22] An acid number of 7.2 was achieved for the VE828 used throughout this thesis. In addition, FTIR was used to determine the extent of reaction. FTIR spectroscopy characterization was performed on a Nicolet 6700 FTIR and can be found in *Figure 20*. In the mid-IR range, 32 cumulative scans were taken at a resolution of 2 cm^{-1}.

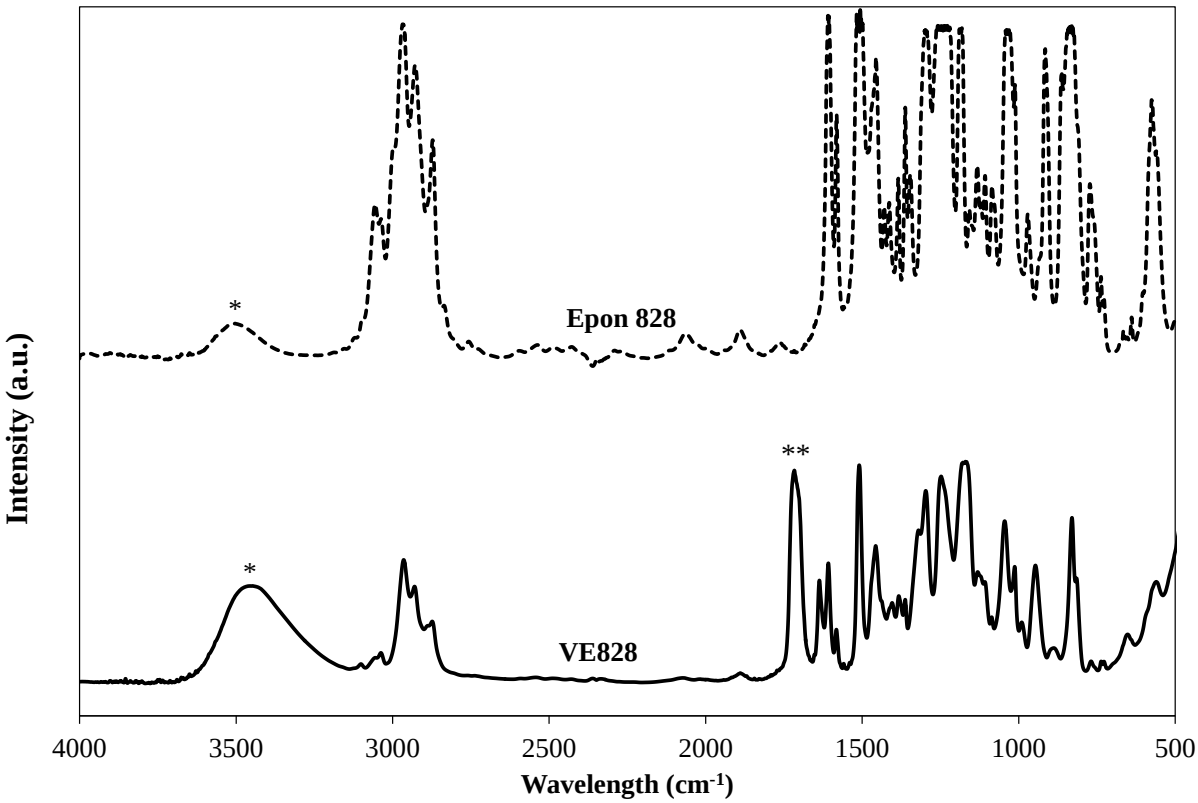

Figure 20. Mid-IR spectra of Epon and VE828 with * representing hydroxyl groups and ** representing carbonyl groups.

Epon 828 and VE828 were further analyzed using gel permeation chromatography (GPC), which can be seen in *Figure 21*. Experiments were performed using a Waters 2695 GPC fitted with Waters Styragel HR4, HR2, and HR1 columns in series using Optima™ THF (1 mL min^{-1}) as the mobile phase. A Waters 2414 Refractive Index Detector was used and GPC samples were prepared at a concentration of 2 mg/mL.

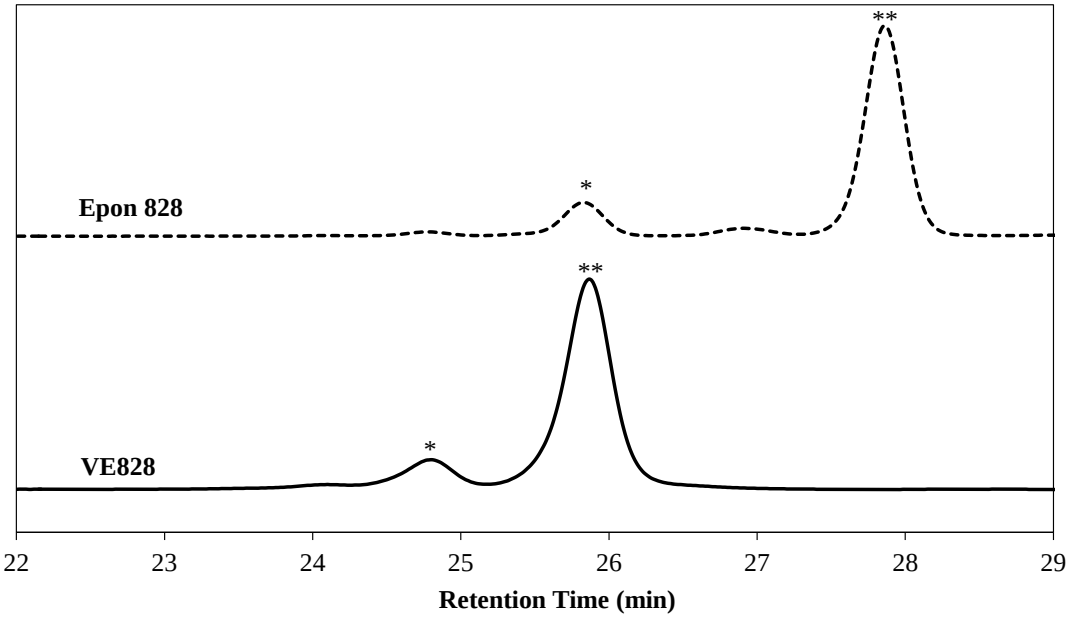

Figure 21. GPC trace for VE828 and Epon 828, with * representing n=1 and ** representing n=0.

Epon 828 has two peaks, with the first peak (25.9 min) being when n = 1 and the second peak (27.9 min) being when n = 0 (refer to *Figure 19*). After methacrylation, the peaks shift forward due to an increase in molecular weight. The absence of a broad peak indicates that homopolymerization of the epoxy functional groups did not occur.[22] The number average molecular weight (M_n) and weight average molecular weight (M_w) of VE828 were determined by comparison to polystyrene standards and through ^{1}H NMR analysis (Table 8). The ^{1}H NMR spectra for VE828 can be found in Appendix A.

Table 8.

Experimentally determined molecular weights of VE828 on the bases of GPC and ^{1}H NMR

Resin	GPC Exp. M_n (g/mol)	GPC Exp. M_w (g/mol)	Exp. ^{1}H NMR M_n (g/mol)	^{1}H NMR n
VE828	654	564	578 g/mol	0.237

The procedure outlined in La Scala *et al.* was used to calculate the M_n of VE828 through ^{1}H NMR analysis.[22] The difference in molecular weights between GPC and ^{1}H NMR is likely due to the GPC polystyrene standard curve. The low molecular weight PS standard at 492 g/mol is a group of peaks that span approximately 3 minutes, which introduces error into the calibration curve. In addition, the VE828 resin may swell differently than polystyrene in THF.[18]

4.2.3 Synthesis of MLMCs. Phenol, guaiacol, and 4-propylguaiacol were methacrylated (*Figure 22*) and purified through aqueous washes and flash chromatography.

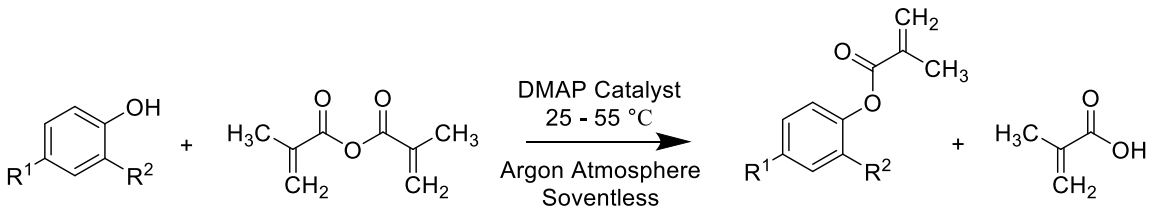

Guaiacol: R^1 = H, R^2 = -OCH_3
Phenol: R^1 = R^2 = H
4-Propylguaiacol: R^1 = -$CH_2CH_2CH_3$, R^2 = -OCH_3

MG: R^1 = H, R^2 = -OCH_3
PM: R^1 = R^2 = H
M4PG: R^1 = -$CH_2CH_2CH_3$, R^2 = -OCH_3

Figure 22. Reaction of lignin model compounds with methacrylic anhydride to produce methacrylated lignin model compound monomers.

In a 500 mL three necked round bottom flask, 50 g of LMC was reacted with 1.05 times the stoichiometric amount of methacrylic anhydride in the presence of DMAP catalyst (2 mol % of methacrylic anhydride). The mixture was purged with argon for approximately 10 minutes in order to remove oxygen and moisture and was subsequently sealed. The mixture was then heated to 55 °C and mixed via stir bar for 24 to 48 hours. Methylene chloride (500 mL) was added to the reaction mixture prior to aqueous washing.

To remove methacrylic acid, unreacted methacrylic anhydride, and unreacted lignin model compounds, the organic phase was washed with a saturated sodium bicarbonate solution until carbon dioxide was no longer formed. The organic phase was washed with sodium hydroxide (2.5M), hydrochloric acid (1M), and water solutions. The MLMCs were then dried over sodium sulfate, filtered, and concentrated under reduced pressure. Flash chromatography is necessary to remove the remainder of impurities in the MLMC products. Flash chromatography was performed on a Grace Reveleris X2 system

using ethyl acetate and hexanes with a 0 to 20 % ethyl acetate gradient with 100g Grace silica columns. MLMC purification is possible through recrystallization, although this separation technique was not used in this study.[85] Industrially, it may be possible to purify the MLMCs through vacuum distillation, which would allow the recovery of methacrylic acid as a potential product.

All MLMCs and VE828 were characterized by ^{1}H NMR (400.13 MHz, 32 scans at 298.2K) and ^{13}C NMR (101 MHz, 256 scans at 298.2K) using a Varian Mercury 400 MHz Nuclear Magnetic Resonance System. The ^{1}H NMR and ^{13}C NMR spectra can be found in the Appendix.

Phenyl Methacrylate (PM). ^{1}H NMR (DMSO-d6): δ 7.46− 7.15 (bm, 5H), 6.28 (t, 1H), 5.90 (t, 1H), 2.00 (s, 3H). ^{13}C NMR (DMSO-d6): δ 162.30, 150.61, 135.32, 129.54, 127.73, 125.88, 121.83, 18.08 ppm.

Methacrylated Guaiacol (MG, 2-Methoxyphenyl Methacrylate). ^{1}H NMR (DMSO-d6): δ 7.28−6.95 (bm, 4H), 6.28 (s, 1H), 5.89 (t,1H), 3.76 (s, 3H), 2.00 (s, 3H). ^{13}C NMR (DMSO-d6): δ 165.17, 151.38, 139.82, 135.49, 128.13, 127.42, 123.32, 121.03, 113.22, 56.15, 18.55 ppm.

Methacrylated-4-Propylguaiacol (M4PG, 4-Propyl-2-methoxyphenol Methacrylate). ^{1}H NMR (DMSO- d6): δ 6.99−6.75 (bm, 3H), 6.25 (s, 1H), 5.86 (t, 1H), 3.74 (s, 3H), 2.55 (t, 2H), 1.60 (m, 2H), 0.91 ppm (t, 3H). ^{13}C NMR (DMSO- d6): δ 164.83, 150.57, 141.23, 137.31, 135.12, 127.49, 122.34, 120.17, 112.76, 55.61, 37.21, 24.21, 18.11, 13.68 ppm.

4.2.4 Resin curing. Each MLMC was mixed with VE828 in a 1:1 weight ratio. Additionally, VE828 was mixed with styrene in a 1:1 weight ratio for use as a standard

equivalent to commercial resins. Each vinyl ester resin was free radically polymerized using Trigonox® 239 (1.5 wt % of total resin mass) as the initiator. The resins were degassed until no visible bubbles remained, transferred into a silicone rubber mold, and purged with argon for 20 minutes. The VE828:St resins were degassed for a shorter period of time to prevent the evaporation of styrene. All resins were cured at 90 °C for 4 hours with a subsequent post cure at 180 °C for 2 hours. The thermosets were allowed to cool to room temperature before removal from the vacuum oven.

4.2.5 Extent of cure. Near-infrared (near-IR) spectra of the uncured and cured VERs were obtained using a Nicolet iS50 FT-IR in order to determine the extent of cure. In the near-IR range, 32 cumulative scans were taken at a resolution of 2 cm^{-1} at room temperature.

The cured thermosets (typically of 3-4 mm thickness) were cleaned with acetone thoroughly and subsequently dried before the near-IR spectra were taken. The VERs were contained in a glass vessel with a thickness of 3 mm when obtaining the near-IR spectra. The extents of cure were determined using Equations 14 and 15 for styrenic vinyl and methacrylate vinyl groups, respectively. Equations 14 and 15 compare the height and/or area of the styrenic vinyl and methacrylate vinyl peaks before and after curing relative to an internal standard that is not affected by the cure. $ABS_{wavelength}$ refers to the peak height at the subscripted wavelength.

$$X = \frac{\left(\frac{ABS_{6135cm^{-1}}}{ABS_{4263cm^{-1}}}\right)_{unreacted} - \left(\frac{ABS_{6135cm^{-1}}}{ABS_{4263cm^{-1}}}\right)_{reacted}}{\left(\frac{ABS_{6135cm^{-1}}}{ABS_{4263cm^{-1}}}\right)_{unreacted}} \tag{14}$$

$$X = \frac{\left(\frac{ABS_{6165cm^{-1}}}{ABS_{4263cm^{-1}}}\right)_{unreacted} - \left(\frac{ABS_{6165cm^{-1}}}{ABS_{4263cm^{-1}}}\right)_{reacted}}{\left(\frac{ABS_{6165cm^{-1}}}{ABS_{4263cm^{-1}}}\right)_{unreacted}} \quad (15)$$

4.2.6 Polymer Properties. DMA was used to determine the thermo-mechanical properties of each thermoset, which includes the glass transition temperature (T_g), storage modulus (E') at 25 °C, rubbery temperature, rubbery E', and effective molecular weight between crosslinks (M_c). M_c was calculated using Equation 16,

$$M_c = \frac{3RT\rho}{E} \quad (16)$$

where R is the ideal gas constant, T is absolute temperature, and ρ is the sample density at room temperature. The rubbery E' and T were defined as the point at which the storage modulus increases with increasing temperature in the rubbery region.[75] The density of the polymer was determined using Archimedes' principle at room temperature.[76] Typical DMA sample dimensions were 35 x 12 x 3 mm^3 and a single cantilever geometry was used. The temperature was increased from 0 to 250 °C at a rate of 2 °C per minute, while oscillating at 1 Hz with a 7.5 µm deflection. A Poissions ratio of 0.35 was used.

4.3 Results and Discussion

4.3.1 Resin characterization. PM, MG, and M4PG are clear, transparent liquids at room temperature both after aqueous purification and flash chromatography purification. The estimated purity of each MLMC after aqueous purification was not determined in this work; however, data adapted from Stanzione's dissertation is shown in Table 9 for comparative purposes.[72] All purities are based on ^{1}H NMR analyses. The

aqueous washing procedure was not optimized and it may be possible to achieve a higher purity than what was achieved.[72]

Table 9.

Purity of MLMCs, on the basis of ^{1}H NMR, after aqueous wash purification[72]

Methacrylated Phenolic	Methacrylated Phenolic (mol %)	Unreacted LMC (mol %)	Methacrylic Anhydride (mol %)	Methacrylic Acid (mol %)	Methacrylated Topanol A (mol %)
PM	92.4 ± 3.0	[a]	1.8 ± 1.2	1.4 ± 1.0	4.5 ± 2.6
MG	80.4 ± 0.4	4.5 ± 2.6	3.6 ± 2.7	3.9 ± 2.7	7.8 ± 2.8
M4PG	82.1 ±1.7	6.8 ± 1.6	0.8 ± 0.2	0.3 ± 0.3	10.1 ± 0.6

[a] The amount of unreacted phenolic cannot be determined through ^{1}H NMR due to overlapping peaks in the aromatic region.[72]

Methacrylated phenol has the highest purity largely due to the fact that the amount of unreacted phenol was not determined through ^{1}H NMR analysis. However, the concentration of unreacted phenol is anticipated to be similar or less than that in MG and M4PG due to the higher reactivity of phenol.[57] After aqueous purification, all MLMCs have a significant amount of methacrylic anhydride, methacrylic acid, and methacrylated topanol A, all of which possess vinyl bonds that will react during the polymerization process. The presence of the unreacted methacrylic anhydride results in additional crosslinking within the polymer network.

The MLMCs were further purified through flash chromatography. All MLMCs required purities greater than 97.5 mol % in order to be used in this study. MLMCs with purities greater than 97.5 mol % are referred to as pure. Table 10 shows the purities of the MLMCs after flash chromatography.

Table 10.

Purity of MLMCs, on the basis of ^{1}H NMR, after aqueous wash and flash chromatography purification

Methacrylated Phenolic	Methacrylated Phenolic (mol %)	Unreacted LMC (mol %)	Methacrylic Anhydride (mol %)	Methacrylic Acid (mol %)	Methacrylated Topanol A (mol %)
PM	99.1 ± 0.2	0	0.3 ± 0.2	0.7 ± 0.0	0
MG	97.8 ± 0.3	0	1.0 ± 0.1	0.4 ± 0.2	0.7 ± 0.4
M4PG	99.4 ± 0.1	0	0.3 ± 0.1	0.33 ± 0.0	0

Flash chromatography removed all unreacted LMCs and greatly reduced the amount of methacrylic anhydride, methacrylic acid, and methacrylated topanol A. The reactive impurities are predicted to be at a low enough concentration that they will not have a significant impact on resin or thermosetting polymer properties. The presence of methacrylic anhydride, methacrylic acid, and methacrylated topanol A in the MLMC product indicates that imperfect separation was achieved in the flash chromatography system. With different solvents, or perhaps a more gradual solvent gradient or step method with multiple column runs, near perfect separation could be achieved. Perfect separation was achieved between the MLMC product and LMC reactant. For the purpose of this study, the achieved purities of each MLMC were deemed acceptable. A GPC chromatogram of PM, MG, and M4PG can be found in Appendix A as an additional confirmation of purity and the absence of oligomers. In addition, the ^{1}H NMR spectra of each pure RD can be found in the Appendix B.

When MLMCs are blended with VE828 in a 1:1 ratio, a resin with a green hue is produced. The green hue is attributed to the AMC-2 catalyst that was used in the synthesis of VE828, which would need to be removed to produce a clear resin for commercial applications. The viscosities of each resin were not determined in this thesis,

but qualitatively the viscosity of the blends increased with increased substituents on the MLMC aromatic ring. Viscosity experiments are recommended for future studies.

4.3.2 Extent of cure. Pictures of pure VE828:MLMC plastics are shown in *Figure 23*.

(a) (b) (c)

Figure 23. Pictures of cured (a) 1:1VE828:PM, (b) 1:1 VE828:MG, (c) 1:1 VE828:M4PG.

FTIR near-IR spectroscopy was used to determine the extent of cure of each resin. *Figure 24* shows the near-IR spectra for 1:1 blends of VE828 and purified PM, MG, and M4PG. The VE828 pure and impure MLMCs blends have similar spectra.[72]

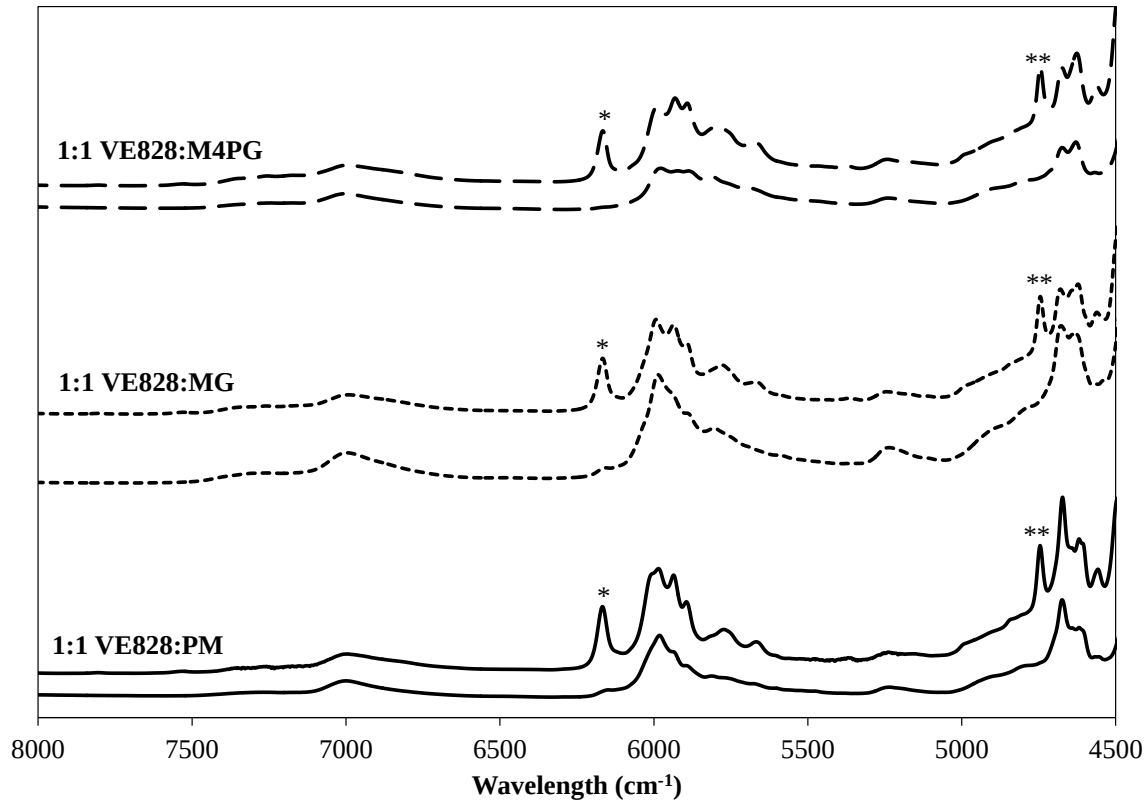

Figure 24. Near-IR spectra for 1:1 blends of VE828 and purified PM, MG, and M4PG. The methacrylate C=C bond peaks are labeled * and the $=CH_2$ peaks are labeled **.

The absorption bands at 6165 cm^{-1} and 4625 cm^{-1} are a result of methacrylate (=C—H) bonds and internal phenyl groups, respectively. The methacrylate (=C—H) bond also absorbs at 4743 cm^{-1}; however, this band was not used to determine the extent of cure due to the sharp baseline drop at nearby wavelengths, which makes peak area calculations unreliable. It can be seen that the methacrylate band at 6265 cm^{-1} decreases during the polymerization, which is a result of the vinyl bonds polymerizing. The extent of cure of VE828 blended with pure and impure reactive diluents is shown in Table 11. The impure

extent of cure data was adapted from Stanzione's dissertation and is used for comparison purposes.[72]

Table 11.

Extent of cure of pure and impure VE828:RD resins

System	Extent of Cure Pure	Extent of Cure Impure[72]
1:1 VE828:St	~100 %	~100 %
1:1 VE828:PM	94 %	94 %
1:1 VE828:MG	95 %	95 %
1:1 VE828:M4PG	99 %	99 %

It can be seen that the impurities (unreacted MLMC, methacrylic anhydride, methacrylic acid, and methacrylated topanol A) do not have an effect on the extent of cure of the resin blends. The impurities may have an effect on cure kinetics (reactivity of the methacrylate vinyl bond) even though the extents of cures are similar.[78] The extent of cure only measures the decrease in methacrylate or styrenic vinyl bonds and does not give information about the composition of the polymer network formed during the cure. Cure kinetic studies are currently being conducted.

4.3.3 Polymer properties. Polymerization of the VE828:St and MLMC blends resulted in visually identical, hard thermosets that were transparent with a green hue. It is anticipated that colorless plastics would be produced if a colorless catalyst and initiator (Trigonox® 239 has a yellow hue) were used. The percent bio-based content was calculated and can be seen in Table 12.[86, 87]

Table 12.

Bio-based content of VE828-based thermosets

System	Bio-Based Content (%)
1:1 VE828:St	0
1:1 VE828:PM	29.7
1:1 VE828:MG	31.9
1:1 VE828:M4PG	36.6

In these calculations, it was assumed that all LMCs were derived from lignin and methacrylic anhydride was derived form a petroleum feedstock. To calculate a percentage, the amount of bio-based carbon in each LMC blend was divided by the amount of total carbon in the LMC blend.[88] VE828 is derived from non-renewable resources.

Thermo-mechanical properties of the resins were measured using DMA. DMA was performed on all pure VE828:MLMC blends, as well as VE828:St for commercial comparison. *Figure 25*, which is data adapted from Stanzione's Ph.D. dissertation for comparative purposes, shows the storage modulus and loss modulus as a function of temperature for the impure 1:1 VE828:RD and 1:1 VE828St blend.[72] Table 13 shows the quantitative thermomechanical properties.[72]

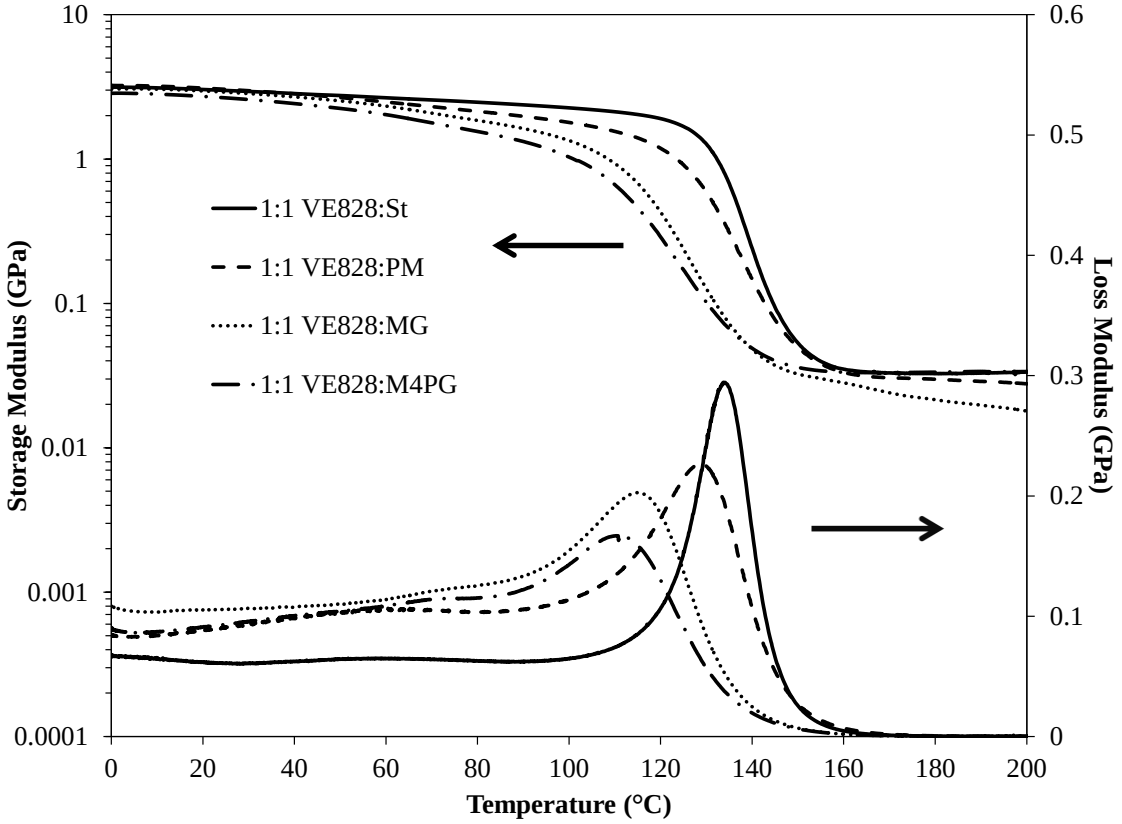

Figure 25. VE828 blends made with impure reactive diluents and styrene for commercial comparison, adapted from Stanzione *et al.*[72]

Table 13.

Thermo-mechanical properties of VE828 blends with impure MLMCs and styrene, adapted from Stanzione et al[72]

Not Pure System	***E′* at 25 (°C)**	***E′(T)* Inflection (°C)**	**Peak of *E″* (°C)**	**Peak of tan *δ* (°C)**	**Rubbery *E′* (MPa)**	**Rubbery *T* (°C)**	**ρ at 25 °C (g cm^{-3})**	**eff. M_C (g mol^{-1})**
1:1 VE828:St	2.9 ± 0.1	133.7 ± 0.9	134.3 ± 0.5	143.0 ± 1.4	29.7 ± 2.4	170.6 ± 0.2	1.132 ± 0.003	424.6 ± 34.8
1:1 VE828:PM	3.0 ± 0.4	129.0 ± 3.4	129.0 ± 4.0	142.0 ± 3.5	28.9 ± 6.2	190.0 ± 14.0	1.214 ± 0.009	485.0 ± 0.0
1:1 VE828:MG	3.1 ± 0.4	118.0 ± 3.4	117.0 ± 4.0	134.0 ± 3.5	24.9 ± 6.2	185.0 ± 14.0	1.228 ± 0.009	564.0 ± 75
1:1 VE828:M4PG	2.7 ± 0.4	111.0 ± 3.4	111.0 ± 4.0	129.0 ± 3.5	33.2 ± 6.2	170.0 ± 14.0	1.183 ± 0.009	401.0 ± 0.0

Figure 26 shows the storage modulus and loss modulus as a function of temperature for the pure 1:1 VE828:RD, as well as styrene for commercial comparison. Table 14 shows the quantitative thermo-mechanical properties for the pure 1:1 VE828:RD blends.

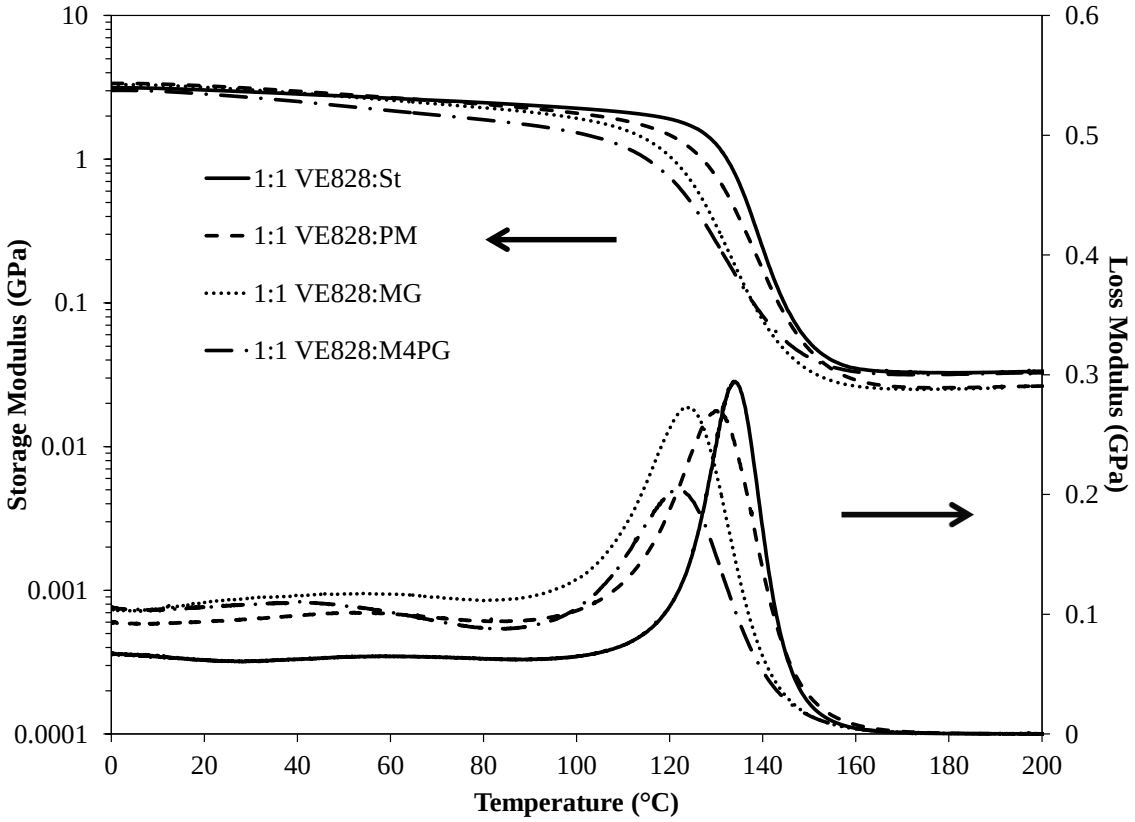

Figure 26. VE828 blends made with pure reactive diluents and styrene for commercial comparison.

Table 14.

Thermo-mechanical properties of VE828 blends with pure MLMCs and styrene

Pure System	***E′* at 25 (°C)**	***E′(T)* Inflection (°C)**	**Peak of *E″* (°C)**	**Peak of tan *δ* (°C)**	**Rubbery *E′* (MPa)**	**Rubbery *T* (°C)**	**ρ at 25 °C (g cm^{-3})**	**eff. M_C (g mol^{-1})**
1:1 VE828:St	2.9 ± 0.1	133.7 ± 0.9	134.3 ± 0.5	143.0 ± 1.4	29.7 ± 2.4	170.6 ± 0.2	1.132 ± 0.003	424.6 ± 34.8
1:1 VE828:PM	3.2 ± 0.1	128.2 ± 2.1	129.4 ± 2.2	142.4 ± 1.7	24.9 ± 1.3	185.2 ± 0.1	1.208 ± 0.003	557.4 ± 29.7
1:1 VE828:MG	3.5 ± 0.1	124.7 ± 1.5	125.9 ± 1.5	139.8 ± 1.8	25.1 ± 0.6	174.8 ± 0.3	1.221 ± 0.001	543.4 ± 12.1
1:1 VE828:M4PG	2.7 ± 0.2	121.8 ± 1.8	123.2 ± 1.8	137.8 ± 1.6	30.8 ± 0.9	171.8 ± 0.1	1.172 ± 0.002	422.3 ± 12.5

Qualitatively, both impure and pure VE828:RD blends have similar thermograms; however, the pure VE828:RD blends tend to have a sharper spike in the loss modulus curve.

Commercial styrene diluted VERs typically have *E′*s greater than 2.0 GPa at 25 °C, which is in agreement with what is reported in Table 13; however, the 1:1 VE828:St *E′* is higher than what is reported by Stanzione *et al.*[12] In general, all pure and impure VE828:MLMC thermosets have a *E′* that is comparable to styrene resins. Also, RD purity does not have a significant effect on the *E′* at 25 °C, with the exception of VE828:MG that has a 0.4 GPa increase. It is expected that the methoxy group would increase the storage modulus due to increased intermolecular interactions, which can be seen when comparing VE828:PM to pure VE828:MG. The methoxy oxygen has been suggested to be a proton acceptor for hydrogen bonding in conjunction to the glycidyl hydroxyl group found on VE828.[79]

Using the theory of rubbery elasticity, the M_cs of each cured resin were determined.[75] The rubbery modulus was defined as the *E′* at the local minimum within the rubbery region. The VE828:M4PG blends showed M_cs that were lower than that of the VE828:St blend; however, the VE828:MG and PM blends had higher effective M_cs than the styrene blend. The increased M_c between VE828:MG/PM and VE828:St can be attributed to the molecular weight gained through the methacrylate group.

Throughout this thesis, all blends have been reported in 1:1 weight ratios; however, looking at the data in terms of molar ratios will give a different perspective. The weight ratios are used for industrial purposes, where a certain weight of RD is added to the VER in order to reduce the viscosity of the blend for production purposes. Table 15

shows the corresponding molar ratios for 1:1 VE828:St, VE828:PM, VE828:MG, and VE828:M4PG.

Table 15.

VE828:RD weight ratio to molar ratio conversion

VE828:RD Weight Ratio	RD MW (g/mol)	VE828:RD Molar Ratio
1:1 VE828:St	104.2	15:85
1:1 VE828:PM	162.2	22:78
1:1 VE828:MG	192.2	25:75
1:1 VE828:M4PG	234.3	29:71

Due to the molecular weight difference of each RD, the molar concentration of RD is not constant and varies from 71 % to 85 %. As stated earlier, the effective M_cs for 1:1 VE828:MG and 1:1 VE828:PM are higher than that of 1:1 VE828:St. Based on the VE828:MLMC molar ratios, there is an increased molar concentration of VE828 as the molecular weight of the RD increases for 1:1 (wt) VE828:RD resins. As the concentration of VE828 increases, the amount of crosslinking in the polymer network increases due to the di-functionality of the VE828 resin. Therefore, 1:1 (wt) VE828:M4PG should have more crosslinks than 1:1 (wt) VE828:MG, which should have more crosslinks than 1:1 (wt) VE828:PM. With an increased crosslinking in the VE828:PM/MG plastics, the effective M_c is expected to decrease. However, the VE828:PM/MG effective M_c is higher than that of styrene, which suggests that the increase in molecular weight of the methacrylate groups has a greater effect on effective M_c than the additional crosslinking in the VE828:PM/MG blends. It is hypothesized that VE828:M4PG has a lower effective M_c than the other VE828:MLMC resins due to

physical interactions of the propyl group, whereby the propyl group hooks on adjacent polymer chains.

Commercial vinyl ester resins that are diluted with styrene typically have T_gs greater than 120 °C.[18, 22, 89] The T_g based on the peak of the E'' curve is similar to that of the inflection point of the E' curve, which is typical among VERs; however, the T_g based on the tan δ curve is higher than that based on the E'' or E' curve.[90, 91] In order to use a more conservative value, the T_g is defined as the peak of the E'' curve.

It can be seen that the T_g trend is the same for the impure and pure reactive diluents; however, the impure MG and M4PG RDs resulted in a substantially lower T_g than the pure analogs. The impure RDs contain unreacted phenolic, methacrylic anhydride, methacrylic acid, and methacrylated topanol A. The unreacted phenolics act as plasticizer and reduce the T_gs of the plastics. Methacrylic anhydride provides additional crosslinking to the polymer network, which would increase the T_g of the polymer. It is believed that impure VE828:PM has a similar T_g to that of pure VE828:PM because of the few unreacted phenol impurities in the resin. Also, it is believed that the significant amount of impurities, specifically the unreacted LMCs, in the MG and M4PG resins caused the substantially lower T_gs.

Based on the pure VE828:MLMC thermosets, it can be seen that the methoxy and proypyl side groups have a marginal effect on the T_g of the resulting polymer. However, the molar ratios of VE828:RD are not constant for each reactive diluent, which will have an effect on the resulting T_g of the plastic. As stated earlier, the increase in the VE828 molar concentration in the VE828:MLMC resins will increase the crosslinking of the plastic. The T_g data shows that even with increased crosslinking in each of the resins, the

T_g still decreases with increased ring substituents. The extent at which the T_g decreases due to ring substituents is greater than that of the T_g increase due to additional crosslinking. In order to determine the true effect of the ring substituents on polymer properties, the VE828:RD resins need to have the same molar VE828:RD ratio. Overall, the data suggests that both PM, MG, and M4PG are effective RD replacements, when pure, for styrene. Also, the impure and pure RDs have a marginal effect on the density of the plastic.

The heterogeneity of a polymer can be qualitatively determined through the broadness of the tan δ thermogram. In addition, a broad tan δ thermogram means that the polymer exhibits a broader glass transition region.[84] For all the VE828-based thermosets, the width of the tan δ peaks qualitatively increased with aromatic side chain functionality on the MLMC, regardless of purity. The tan δ thermograms are shown in *Figure 27* and *Figure 28*. *Figure 27* contains data adapted from Stanzione's Ph.D. dissertation for comparative purposes.[72]

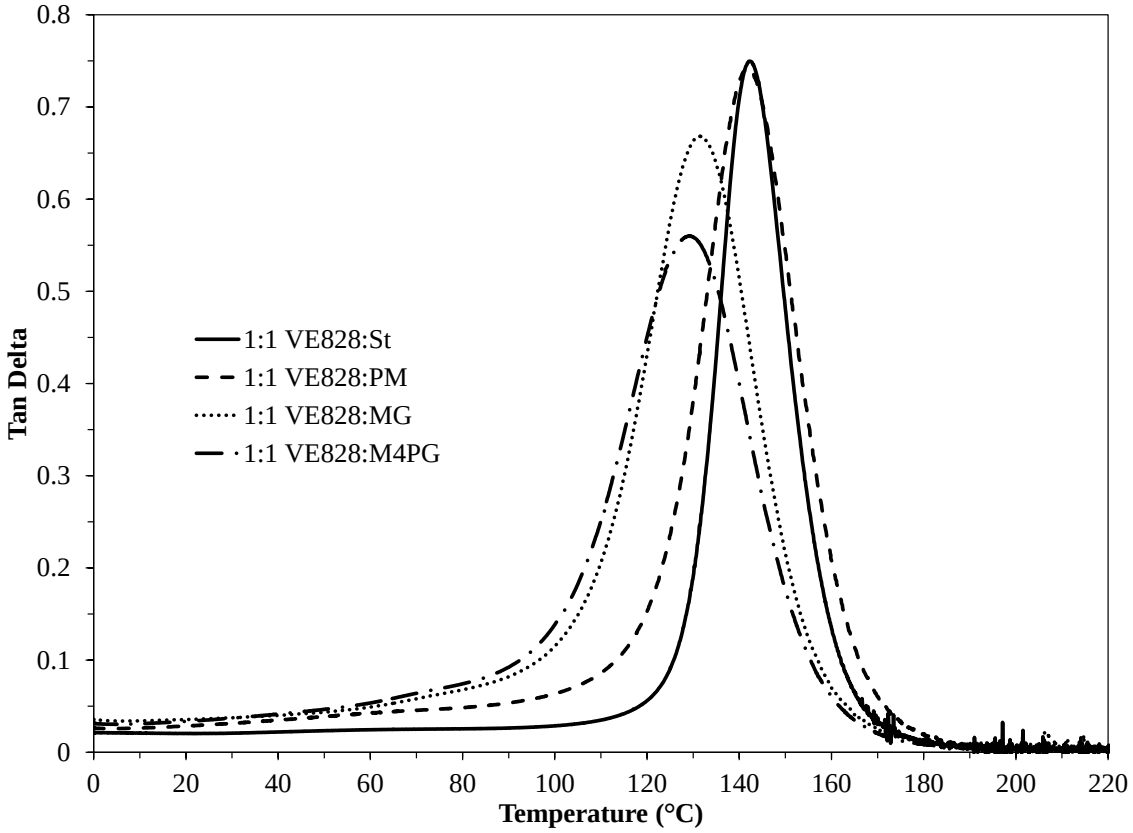

Figure 27. The tan δ of VE828 resins diluted with impure MLMCs and styrene is shown as function of temperature, adapted from Stanzione *et al*.[72]

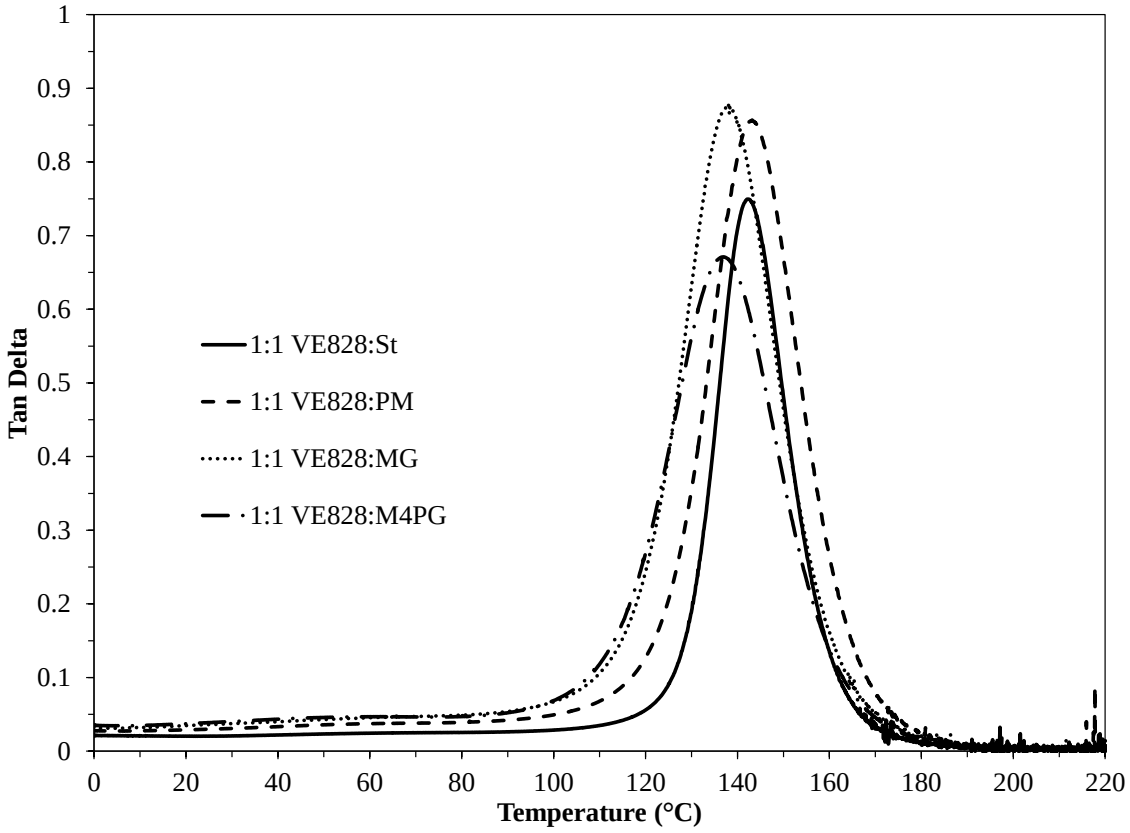

Figure 28. The tan δ of VE828 resins diluted with pure MLMCs and styrene is shown as function of temperature.

For impure VE828:RD plastics, the height of the tan δ curve, which is an indication of viscous/elastic behavior, decreases with increased ring substituents. This trend was not observed in the pure VE828:RD plastics. In addition, it was found in Chapter 3 that as the number of MBO crosslinking agents increased, the height of the tan δ curve decreased; however, this trend was not observed in the pure VE828:RD resins.

4.4 Conclusions

In this study, three lignin model compounds (phenol, guaiacol, and 4-propylguaiacol) were methacrylated via an esterification reaction with methacrylic

anhydride. PM, MG, and M4PG were shown to be suitable reactive diluent replacements for styrene in vinyl ester resins. Pure MLMCs were blended in 1:1 weight ratios with a commercial vinyl ester resin (VE828) and compared to data from Stanzione *et al.[72]* The pure MLMCs, when blended with VE828, produced thermosets with comparable T_g values to that of VE828 blended with styrene. The impure MLMCs had T_g values that were inferior to VE828 blended with styrene, with the exception of impure PM. This work shows that purity and ring substituents of the reactive diluents affect the polymer properties in VE resins. Cure kinetics, fracture toughness, and flexural strength tests are currently being conducted with all MLMCs to determine the effect of both purity and functional groups on polymer properties. Overall, all pure MLMCs were successfully used as reactive diluents in vinyl ester resins; however, increasing the purity of the MLMCs yields more desired thermomechanical properties when cured.

Chapter 5

Conclusions and Recommendations

5.1 Conclusions

The use of lignin as a feedstock for sustainable vinyl ester thermosetting plastics was investigated in this thesis. Lignin is a highly aromatic polymer that is produced in excess $50x10^6$ tons annually, which makes it an attractive feedstock for high value applications (thermosetting plastics). With increased attention in academia and industry to the depolymerization of lignin, especially via fast pyrolysis, research needs to be done on profitable applications for lignin depolymerization products (lignin-derived bio-oils).

In Chapter 3, the use of lignin-derived bio-oils as a feedstock for vinyl ester resins was investigated. Three representative lignin-derived bio-oil mimics were made based on five literature sources and were methacrylated to produce vinyl ester resins. The first bio-oil mimic was based upon four sources, the second was based upon five sources, and the third was based upon Choi *et. al.*[26, 30-33] Each resin contained the same classes of molecules (phenols, guaiacols, catechols); however, there were variations between each. Most notably, the bio-oil mimic based upon Choi *et. al.* had a low concentration of crosslinking monomers, whereas bio-oil 1 and bio-oil 2 had a significantly higher amount of crosslinking monomers. Curing resulted in hard, transparent plastics with properties similar to that of commercial vinyl ester resins. The glass transition temperature of bio-oil 1 and 2 were approximately 20 °C higher than bio-oil 3, likely do to the decreased concentration of crosslinking monomers present in bio-oil 3. This work showed that high quality lignin-derived bio-oils can be methacrylated as is to produce vinyl ester resins that can be cured into plastics with desirable thermomechanical properties.

In addition, the uses of lignin model compounds (phenol, guaiacol, and 4-propylguaiacol) to produce reactive diluents in vinyl ester resins were investigated. All reactive diluents were purified to a concentration greater than 97.5 mol % in order to investigate the effects of ring substituents on polymer properties. The reactive diluents were mixed with a commercial vinyl ester resin to produce a qualitatively low viscosity solution. Curing resulted in plastics with properties similar to that of styrene diluted vinyl ester resins. Also, it was found that ring substituents (methoxy and propyl) on pure methacrylate reactive diluents have little effect on the T_g of 1:1 (wt) VE828:Methacrylated lignin model compound (MLMC) polymers, which is in contrast to what was found by Stanzione when impure reactive diluents were used.

5.2 Recommendations

Throughout this work, flexural and fractural tests were not conducted due to instrument limitations. In addition, viscosity experiments were not performed. In future studies, it would be beneficial to perform these tests in order to further characterize both the resin and plastic. Fractural and flexural tests would provide insight into the strength and toughness of the plastics, in addition to structure property relationships. Viscosity testing is needed in order to determine industrial processing capabilities. Generally, the methacrylated bio-oil and VE828:MLMC resins need to have a viscosity that is within a 200 – 1000 cP range.[28, 92] Too low of a viscosity can cause bubble formation and too high of a viscosity can cause increased injection time and ineffective fiber wetting.[28, 92] In addition, vinyl ester resins are often used in composite applications.[19] The MLMC resins proposed in this thesis could be incorporated into glass fibers, aramid fibers, and carbon fibers, for example. Also, cure kinetic studies are recommended in

order to monitor and potentially optimize the curing procedure. In regard to DMA, it is recommended that thicker samples (5-5.5 mm) be used for analyses in the rubbery region. Thicker sample may give a more accurate depiction of the rubbery region, and thus provide greater accuracy when calculating M_c values.[93]

Relating to the work presented in Chapter 3, future experiments could include the synthesis of a MLMC bio-oil mixture through the one-pot two-step reaction proposed in Stanzione *et al*.[13] The one-pot two-step reaction utilizes methacrylic anhydride to methacrylate the LMCs and subsequently converts the methacrylic acid byproduct into a crosslinking agent.[13] It is hypothesized that this would increase the T_g of the MBO plastic due to additional crosslinking; however, the fractural and flexural properties of the plastic may decrease. Future experiments could also include the purification and methacrylation of a lignin-derived bio-oil that was recently received, in addition to incorporating the previously excluded syringol and 5-hydroxyvanillin phenolics into the bio-oil mimics.

Relating to the work presented in Chapter 4, it would be interesting to determine the magnitude of the effect of the methoxy and propyl substituent groups by keeping the VE828:MLMC molar ratios constant. Although the general effects of the substituents were determined in this work, further experimentation is necessary to determine the extent at which the physical properties are effected. Also, future experiments could include varying the concentration of the MLMCs in the VE828 resins for further characterization of the VE828:MLMC systems.

References

[1] B. Kamm, P. R. Gruber, and M. Kamm, *Biorefineries - Industrial Processes and Products : Status Quo and Future Directions*. Weinheim: Wiley-VCH, 2006.

[2] S.-T. Yang, *Bioprocessing for Value-Added Products from Renewable Resources: New Technologies and Applications* vol. Firstition. Amsterdam; Boston: Elsevier, 2007.

[3] P. J. De Wild, W. J. J. Huijgen, and R. J. A. Gosselink, "Lignin pyrolysis for profitable lignocellulosic biorefineries," *Biofuels Bioproducts & Biorefining-Biofpr,* vol. 8, pp. 645-657, Sep-Oct 2014.

[4] A. Abe, K. Dušek, S. Kobayashi, and S. Błażewicz, *Biopolymers: Lignin, Proteins, Bioactive Nanocomposites* vol. 232; 232. Berlin: Springer, 2010.

[5] E. Ten and W. Vermerris, "Recent developments in polymers derived from industrial lignin," *Journal of Applied Polymer Science,* vol. 132, pp. n/a-n/a, 2015.

[6] D. Schorr, P. N. Diouf, and T. Stevanovic, "Evaluation of industrial lignins for biocomposites production," *Industrial Crops and Products,* vol. 52, pp. 65-73, 2014.

[7] J. F. Stanzione, J. M. Sadler, J. J. La Scala, and R. P. Wool, "Lignin Model Compounds as Bio-Based Reactive Diluents for Liquid Molding Resins," *ChemSusChem,* vol. 5, pp. 1291-1297, 2012.

[8] J. F. Stanzione, J. M. Sadler, J. J. La Scala, and R. P. Wool, "Lignin-derived monomers utilized in biobased resins," *Abstracts of Papers of the American Chemical Society,* vol. 243, Mar 25 2012.

[9] F. Souto, V. Calado, and N. Pereira, "Carbon fiber from lignin: a literature review," *Materia-Rio-De Janeiro,* vol. 20, pp. 100-114, 2015.

[10] E. A. B. d. Silva, M. Zabkova, J. D. Araújo, C. A. Cateto, M. F. Barreiro, M. N. Belgacem, *et al.*, "An integrated process to produce vanillin and lignin-based polyurethanes from Kraft lignin," *Chemical Engineering Research and Design,* vol. 87, pp. 1276-1292, 2009.

[11] I. Brodin, E. Sjöholm, and G. Gellerstedt, "Kraft lignin as feedstock for chemical products: The effects of membrane filtration," *Holzforschung,* vol. 63, pp. 290-297, 2009.

[12] J. F. Stanzione, P. A. Giangiulio, J. M. Sadler, J. J. La Scala, and R. P. Wool, "Lignin-Based Bio-Oil Mimic as Biobased Resin for Composite Applications," *ACS Sustainable Chemistry & Engineering*, vol. 1, pp. 419-426, Apr 2013.

[13] J. F. Stanzione, J. M. Sadler, J. J. La Scala, K. H. Reno, and R. P. Wool, "Vanillin-based resin for use in composite applications," *Green Chemistry*, vol. 14, pp. 2346-2352, 2012.

[14] E. D. Hernandez, "Synthesis and characterization of vanillyl alcohol based thermosetting epoxy resins," Dissertation/Thesis, Rowan University, 2015.

[15] H. A. Wittcoff, B. G. Reuben, and J. S. Plotkin, *Industrial Organic Chemicals*, 3rd ed. Hoboken, N.J.: Wiley, 2013.

[16] R. A. Pethrick, *Polymer Science and Technology: for Engineers and Scientists*. Dunbeath; Glasgow: Whittles Publishing, 2009.

[17] M. J. Forrest, I. ebrary, and L. Rapra Technology, *Analysis of Thermoset Materials, Precursors and Products* vol. 162.; 162; 14, no. 6, 2003; 14, no. 6, 2003. Shrewsbury, U.K: Rapra Technology, 2003.

[18] J. J. La Scala, J. A. Orlicki, C. Winston, E. J. Robinette, J. M. Sands, and G. R. Palmese, "The use of bimodal blends of vinyl ester monomers to improve resin processing and toughen polymer properties," *Polymer*, vol. 46, pp. 2908-2921, Apr 15 2005.

[19] S. Jaswal and B. Gaur, "New trends in vinyl ester resins," *Reviews in Chemical Engineering*, vol. 30, pp. 567-581, Dec 2014.

[20] P. N. Shah, N. Kim, Z. R. Huang, M. Jayamanna, A. Kokil, A. Pine, *et al.*, "Environmentally benign synthesis of vinyl ester resin from biowaste glycerin," *RSC Advances*, vol. 5, pp. 38673-38679, 2015.

[21] S. Agrawal, A. Mishra, and J. S. P. Rai, "Effect of diluents on the curing behavior of vinyl ester resin," *Journal of Applied Polymer Science*, vol. 87, pp. 1948-1951, Mar 21 2003.

[22] J. J. La Scala, J. M. Sands, J. A. Orlicki, E. J. Robinette, and G. R. Palmese, "Fatty acid-based monomers as styrene replacements for liquid molding resins," *Polymer*, vol. 45, pp. 7729-7737, Oct 13 2004.

[23] J. H. Lora and W. G. Glasser, "Recent Industrial Applications of Lignin: A Sustainable Alternative to Nonrenewable Materials," *Journal of Polymers and the Environment*, vol. 10, pp. 39-48, 2002.

[24] T. Voitl and P. R. Von Rohr, "Oxidation of lignin using aqueous polyoxometalates in the presence of alcohols," *ChemSusChem,* vol. 1, pp. 763-769, 2008.

[25] M. N. Belgacem and A. Gandini, *Monomers, Polymers and Composites from Renewable Resources*, 2008.

[26] S. Farag, D. B. Fu, P. G. Jessop, and J. Chaouki, "Detailed compositional analysis and structural investigation of a bio-oil from microwave pyrolysis of kraft lignin," *Journal of Analytical and Applied Pyrolysis,* vol. 109, pp. 249-257, Sep 2014.

[27] F. S. Chakar and A. J. Ragauskas, "Review of current and future softwood kraft lignin process chemistry," *Industrial Crops and Products,* vol. 20, pp. 131-141, Sep 2004.

[28] R. Wool and X. S. Sun, *Bio-Based Polymers and Composites*, 1 ed. Burlington, MA: Elsevier Academic Press, 2005.

[29] S. Jia, B. J. Cox, X. Guo, Z. C. Zhang, and J. G. Ekerdt, "Cleaving the β□O□4 Bonds of Lignin Model Compounds in an Acidic Ionic Liquid, 1-H-3-Methylimidazolium Chloride: An Optional Strategy for the Degradation of Lignin," *ChemSusChem,* vol. 3, pp. 1078-1084, 2010.

[30] H. S. Choi and D. Meier, "Fast pyrolysis of Kraft lignin-Vapor cracking over various fixed-bed catalysts," *Journal of Analytical and Applied Pyrolysis,* vol. 100, pp. 207-212, Mar 2013.

[31] D. K. Shen, S. Gu, K. H. Luo, S. R. Wang, and M. X. Fang, "The pyrolytic degradation of wood-derived lignin from pulping process," *Bioresource Technology,* vol. 101, pp. 6136-6146, Aug 2010.

[32] G. Z. Jiang, D. J. Nowakowski, and A. V. Bridgwater, "Effect of the Temperature on the Composition of Lignin Pyrolysis Products," *Energy & Fuels,* vol. 24, pp. 4470-4475, Aug 2010.

[33] H. E. Jegers and M. T. Klein, "Primary and Secondary Lignin Pyrolysis Reaction Pathways," *Industrial & Engineering Chemistry Process Design and Development,* vol. 24, pp. 173-183, 1985.

[34] M. Hocking, "Vanillin: Synthetic flavoring from spent sulfite liquor (vol 74, pg 1055, 1997)," *Journal of Chemical Education,* vol. 74, pp. 1384-1384, Dec 1997.

[35] E. A. B. da Silva, M. Zabkova, J. D. Araujo, C. A. Cateto, M. F. Barreiro, M. N. Belgacem, *et al.*, "An integrated process to produce vanillin and lignin-based polyurethanes from Kraft lignin," *Chemical Engineering Research & Design,* vol. 87, pp. 1276-1292, Sep 2009.

[36] M. J. de la Torre, A. Moral, M. D. Hernandez, E. Cabeza, and A. Tijero, "Organosolv lignin for biofuel," *Industrial Crops and Products,* vol. 45, pp. 58-63, Feb 2013.

[37] W. Mu, H. X. Ben, A. Ragauskas, and Y. L. Deng, "Lignin Pyrolysis Components and Upgrading-Technology Review," *Bioenergy Research,* vol. 6, pp. 1183-1204, Dec 2013.

[38] A. T. Martinez, F. J. Ruiz-Duenas, M. J. Martinez, J. C. del Rio, and A. Gutierrez, "Enzymatic delignification of plant cell wall: from nature to mill," *Current Opinion in Biotechnology,* vol. 20, pp. 348-357, Jun 2009.

[39] S. Camarero, D. Ibarra, A. T. Martinez, J. Romero, A. Gutierrez, and J. C. del Rio, "Paper pulp delignification using laccase and natural mediators," *Enzyme and Microbial Technology,* vol. 40, pp. 1264-1271, Apr 3 2007.

[40] D. Ibarra, J. Romero, M. J. Martinez, A. T. Martinez, and S. Camarero, "Exploring the enzymatic parameters for optimal delignification of eucalypt pulp by laccase-mediator," *Enzyme and Microbial Technology,* vol. 39, pp. 1319-1327, Oct 3 2006.

[41] D. Stewart, "Lignin as a base material for materials applications: Chemistry, application and economics," *Industrial Crops and Products,* vol. 27, pp. 202-207, Mar 2008.

[42] D. Shen, J. Zhao, R. Xiao, and S. Gu, "Production of aromatic monomers from catalytic pyrolysis of black-liquor lignin," *Journal of Analytical and Applied Pyrolysis,* vol. 111, pp. 47-54, Jan 2015.

[43] R. Lou, S. B. Wu, and G. J. Lyu, "Quantified monophenols in the bio-oil derived from lignin fast pyrolysis," *Journal of Analytical and Applied Pyrolysis,* vol. 111, pp. 27-32, Jan 2015.

[44] F. X. Collard and J. Blin, "A review on pyrolysis of biomass constituents: Mechanisms and composition of the products obtained from the conversion of cellulose, hemicelluloses and lignin," *Renewable & Sustainable Energy Reviews,* vol. 38, pp. 594-608, Oct 2014.

[45] A. K. Deepa and P. L. Dhepe, "Lignin Depolymerization into Aromatic Monomers over Solid Acid Catalysts," *ACS Catalysis,* vol. 5, pp. 365-379, Jan 2015.

[46] B. S. Li, W. Lv, Q. Zhang, T. J. Wang, and L. L. Ma, "Pyrolysis and catalytic pyrolysis of industrial lignins by TG-FTIR: Kinetics and products," *Journal of Analytical and Applied Pyrolysis,* vol. 108, pp. 295-300, Jul 2014.

[47] Q. Bu, H. W. Lei, L. Wang, G. Yadavalli, Y. Wei, X. S. Zhang, *et al.*, "Biofuel production from catalytic microwave pyrolysis of Douglas fir pellets over ferrum-modified activated carbon catalyst," *Journal of Analytical and Applied Pyrolysis,* vol. 112, pp. 74-79, Mar 2015.

[48] S. Brand and J. Kim, "Liquefaction of major lignocellulosic biomass constituents in supercritical ethanol," *Energy,* vol. 80, pp. 64-74, Feb 1 2015.

[49] V. B. F. Custodis, P. Hemberger, Z. Q. Ma, and J. A. van Bokhoven, "Mechanism of Fast Pyrolysis of Lignin: Studying Model Compounds," *Journal of Physical Chemistry B,* vol. 118, pp. 8524-8531, Jul 24 2014.

[50] X. F. Cao, L. X. Zhong, X. W. Peng, S. N. Sun, S. M. Li, S. J. Liu, *et al.*, "Comparative study of the pyrolysis of lignocellulose and its major components: Characterization and overall distribution of their biochars and volatiles," *Bioresource Technology,* vol. 155, pp. 21-27, Mar 2014.

[51] M. Brebu, T. Tamminen, and I. Spiridon, "Thermal degradation of various lignins by TG-MS/FTIR and Py-GC-MS," *Journal of Analytical and Applied Pyrolysis,* vol. 104, pp. 531-539, Nov 2013.

[52] H. X. Ben and A. J. Ragauskas, "Comparison for the compositions of fast and slow pyrolysis oils by NMR characterization," *Bioresource Technology,* vol. 147, pp. 577-584, Nov 2013.

[53] Q. Bu, H. W. Lei, S. J. Ren, L. Wang, Q. Zhang, J. Tang, *et al.*, "Production of phenols and biofuels by catalytic microwave pyrolysis of lignocellulosic biomass," *Bioresource Technology,* vol. 108, pp. 274-279, Mar 2012.

[54] A. M. Azeez, D. Meier, J. Odermatt, and T. Willner, "Fast Pyrolysis of African and European Lignocellulosic Biomasses Using Py-GC/MS and Fluidized Bed Reactor," *Energy & Fuels,* vol. 24, pp. 2078-2085, Mar 2010.

[55] R. Bayerbach and D. Meier, "Characterization of the water-insoluble fraction from fast pyrolysis liquids (pyrolytic lignin). Part IV: Structure elucidation of oligomeric molecules," *Journal of Analytical and Applied Pyrolysis,* vol. 85, pp. 98-107, May 2009.

[56] M. Garcia-Perez, S. Wang, J. Shen, M. Rhodes, W. J. Lee, and C. Z. Li, "Effects of temperature on the formation of lignin-derived oligomers during the fast pyrolysis of Mallee woody biomass," *Energy & Fuels,* vol. 22, pp. 2022-2032, May-Jun 2008.

[57] W. H. Brown and T. Poon, *Introduction to Organic Chemistry,* 4th ed. Hoboken, NJ: Wiley, 2011.

[58] W. H. Brown. (2000). *Introduction to Organic Chemistry (2nd ed.)*.

[59] L. G. Wade, *Organic Chemistry*, 7th ed. Upper Saddle River, NJ: Pearson Prentice Hall, 2010.

[60] O. J. Rees, *Fourier Transform Infrared Spectroscopy : Developments, Techniques, and Applications*. New York: Nova Science Publishers, 2010.

[61] D. A. Skoog, F. J. Holler, and S. R. Crouch, *Principles of instrumental analysis*, 6th ed. Belmont, CA: Thomson Brooks/Cole, 2007.

[62] J. R. Fried, *Polymer Science and Technology*, 2nd ed. Upper Saddle River, NJ: Prentice Hall Professional Technical Reference, 2003.

[63] S. R. Sandler, *Polymer Synthesis and Characterization : A Laboratory Manual*. San Diego: Academic Press, 1998.

[64] K. P. Menard, *Dynamic Mechanical Analysis: A Practical Introduction*: CRC Press, 1999.

[65] L. H. Sperling, *Introduction to Physical Polymer Science*, 4th ed. Hoboken, N.J.: Wiley, 2006.

[66] R. K. Sharma and N. N. Bakhshi, "Upgrading of Pyrolytic Lignin Fraction of Fast Pyrolysis Oil to Hydrocarbon Fuels over Hzsm-S in a Dual Reactor System," *Fuel Processing Technology*, vol. 35, pp. 201-218, Oct 1993.

[67] C. A. Mullen and A. A. Boateng, "Catalytic pyrolysis-GC/MS of lignin from several sources," *Fuel Processing Technology*, vol. 91, pp. 1446-1458, Nov 2010.

[68] R. French and S. Czernik, "Catalytic pyrolysis of biomass for biofuels production," *Fuel Processing Technology*, vol. 91, pp. 25-32, Jan 2010.

[69] L. Devi, K. J. Ptasinski, and F. J. J. G. Janssen, "A review of the primary measures for tar elimination in biomass gasification processes," *Biomass & Bioenergy*, vol. 24, pp. 125-140, 2003.

[70] A. P. Griset, J. Walpole, R. Liu, A. Gaffey, Y. L. Colson, and M. W. Grinstaff, "Expansile Nanoparticles: Synthesis, Characterization, and in Vivo Efficacy of an Acid-Responsive Polymeric Drug Delivery System," *Journal of the American Chemical Society*, vol. 131, pp. 2469-+, Feb 25 2009.

[71] J. Lukaszczyk, B. Janicki, J. Kozuch, and H. Wojdyla, "Synthesis and Characterization of Low Viscosity Dimethacrylic Resin Based on Isosorbide," *Journal of Applied Polymer Science*, vol. 130, pp. 2514-2522, Nov 15 2013.

[72] J. F. Stanzione, III, "Lignin-based monomers: Utilization in high-performance polymers and the effects of their structures on polymer properties," Dissertation/Thesis, University of Delaware, 2013.

[73] Z. H. Guo, H. F. Lin, A. B. Karki, S. Y. Wei, D. P. Young, S. Park, *et al.*, "Facile monomer stabilization approach to fabricate iron/vinyl ester resin nanocomposites," *Composites Science and Technology,* vol. 68, pp. 2551-2556, Sep 2008.

[74] M. A. Stone, B. K. Fink, T. A. Bogetti, and J. W. Gillespie, "Thermo-chemical response of vinyl-ester resin," *Polymer Engineering and Science,* vol. 40, pp. 2489-2497, Dec 2000.

[75] P. J. Flory, *Principles of Polymer Chemistry*. Ithaca,: Cornell University Press, 1953.

[76] W. Noll, "Method for Determining the Density of a Wood Block, Using Archimedes' Principle," *American Journal of Physics,* vol. 25, pp. 39-39, 1957.

[77] L. Rojo, B. Vazquez, J. Parra, A. López Bravo, S. Deb, and J. San Roman, "From natural products to polymeric derivatives of "eugenol": a new approach for preparation of dental composites and orthopedic bone cements," *Biomacromolecules,* vol. 7, pp. 2751-2761, 2006.

[78] T. F. Scott, W. D. Cook, and J. S. Forsythe, "Kinetics and network structure of thermally cured vinyl ester resins," *European Polymer Journal,* vol. 38, pp. 705-716, Apr 2002.

[79] M. Palusiak and S. J. Grabowski, "Methoxy group as an acceptor of proton in hydrogen bonds," *Journal of Molecular Structure,* vol. 642, pp. 97-104, Dec 4 2002.

[80] A. Sanz, A. Nogales, T. A. Ezquerra, N. Lotti, and L. Finelli, "Cooperativity of the beta-relaxations in aromatic polymers," *Physical Review E,* vol. 70, Aug 2004.

[81] T. Ohya and T. Otsu, "Head-to-Head Vinyl-Polymers .10. Cyclo-Polymerization of Ortho-Dimethacryloyloxybenzene," *Journal of Polymer Science Part a-Polymer Chemistry,* vol. 21, pp. 3169-3180, 1983.

[82] S. Ziaee and G. R. Palmese, "Effects of temperature on cure kinetics and mechanical properties of vinyl-ester resins," *Journal of Polymer Science Part B-Polymer Physics,* vol. 37, pp. 725-744, Apr 1 1999.

[83] R. P. Brill and G. R. Palmese, "An investigation of vinyl-ester - Styrene bulk copolymerization cure kinetics using Fourier transform infrared spectroscopy," *Journal of Applied Polymer Science,* vol. 76, pp. 1572-1582, Jun 6 2000.

[84] J. Park, J. Eslick, Q. Ye, A. Misra, and P. Spencer, "The influence of chemical structure on the properties in methacrylate-based dentin adhesives," *Dental Materials*, vol. 27, pp. 1086-1093, Nov 2011.

[85] A. L. Holmberg, J. F. Stanzione, R. P. Wool, and T. H. Epps, "A Facile Method for Generating Designer Block Copolymers from Functionalized Lignin Model Compounds," *ACS Sustainable Chemistry & Engineering*, vol. 2, pp. 569-573, Apr 2014.

[86] P. T. Anastas and J. C. Warner, *Green Chemistry : Theory and Practice*. Oxford England ; New York: Oxford University Press, 1998.

[87] P. T. Anastas and J. B. Zimmerman, "Design through the 12 principles of green engineering," *Environ Sci Technol*, vol. 37, pp. 94A-101A, Mar 1 2003.

[88] U. S. C. House., "Food, Conservation, and Energy Act of 2008," ed. Washington: U.S. G.P.O., 2008.

[89] W. D. Cook, T. F. Scott, S. Quay-Thevenon, and J. S. Forsythe, "Dynamic mechanical thermal analysis of thermally stable and thermally reactive network polymers," *Journal of Applied Polymer Science*, vol. 93, pp. 1348-1359, Aug 5 2004.

[90] J. J. La Scala, M. S. Logan, J. M. Sands, and G. R. Palmese, "Composites based on bimodal vinyl ester resins with low hazardous air pollutant contents," *Composites Science and Technology*, vol. 68, pp. 1869-1876, Jun 2008.

[91] G. R. Palmese and R. L. Mccullough, "Effect of Epoxy Amine Stoichiometry on Cured Resin Material Properties," *Journal of Applied Polymer Science*, vol. 46, pp. 1863-1873, Dec 5 1992.

[92] J. J. LaScala, "The effects of triglyceride structure on the properties of plant oil-based resins," Dissertation/Thesis, ProQuest Dissertations Publishing, 2002.

[93] I. M. McAninch, G. R. Palmese, J. L. Lenhart, and J. J. La Scala, "DMA testing of epoxy resins: The importance of dimensions," *Polymer Engineering & Science*, pp. n/a-n/a, 2015.

Appendix A

^{1}H NMR Spectra

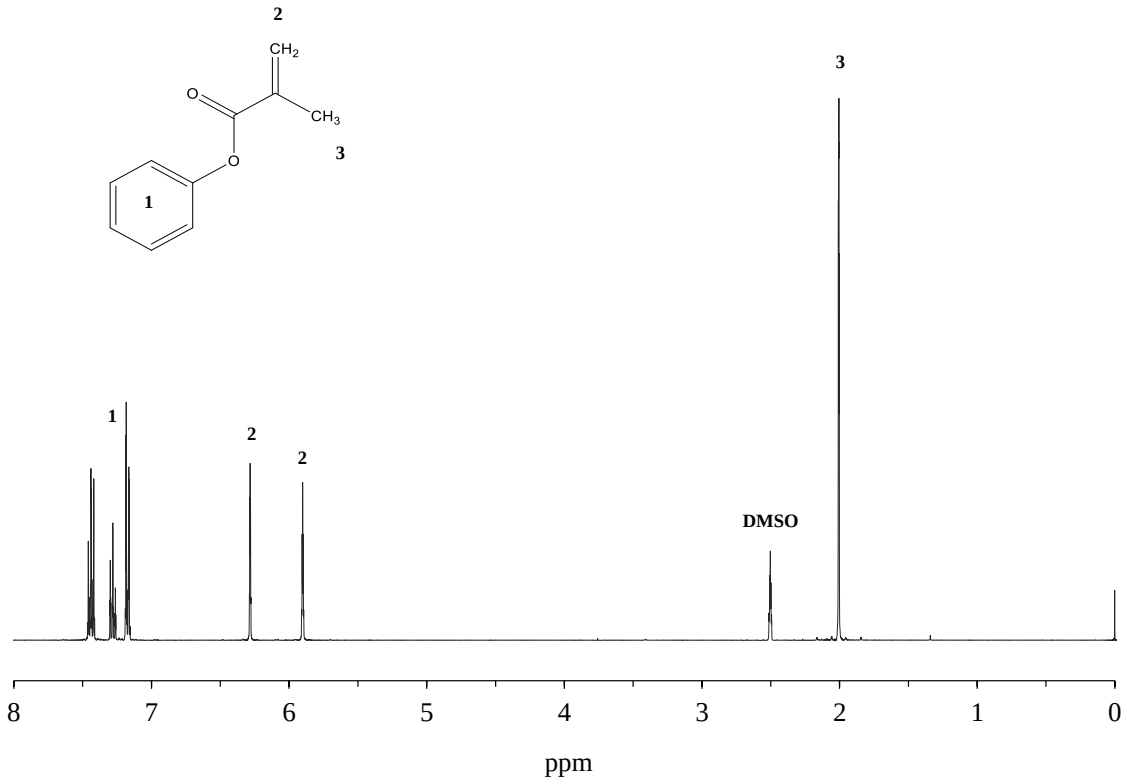

Figure 29. ^{1}H NMR spectra of pure (>97.5 mol %) phenol methacrylate.

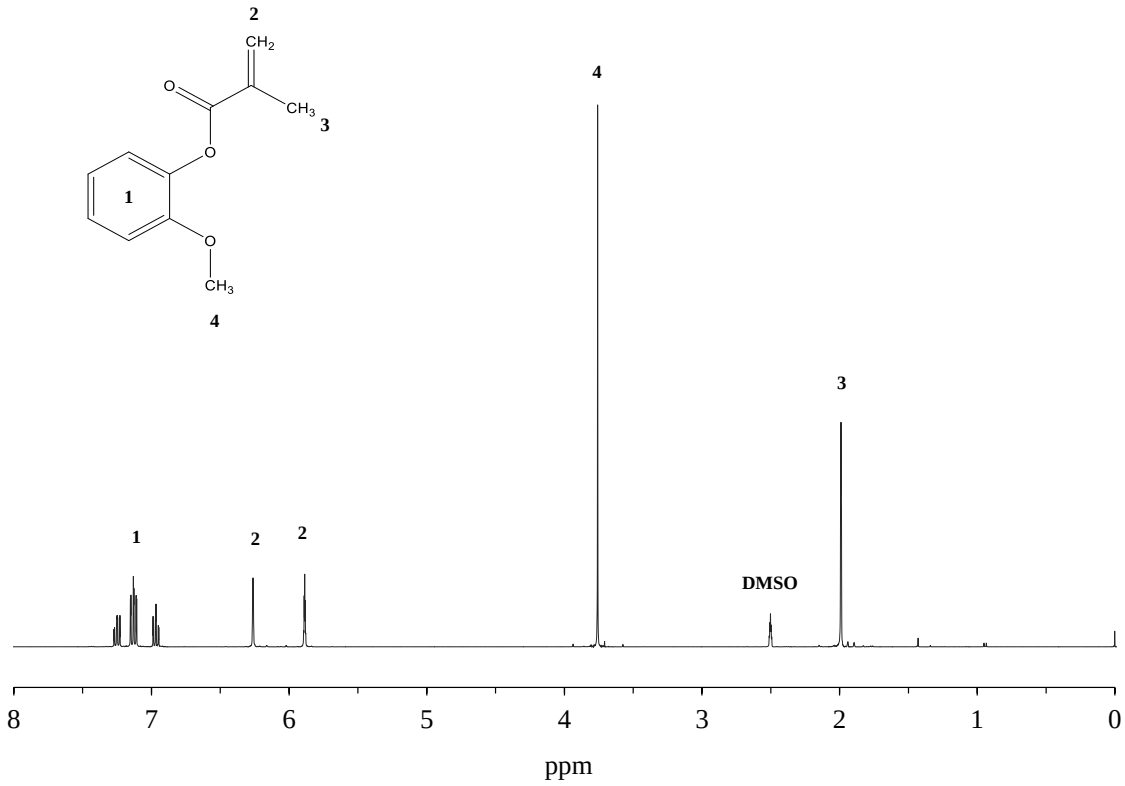

Figure 30. ^{1}H NMR spectra of pure (>97.5 mol %) methacrylated guaiacol.

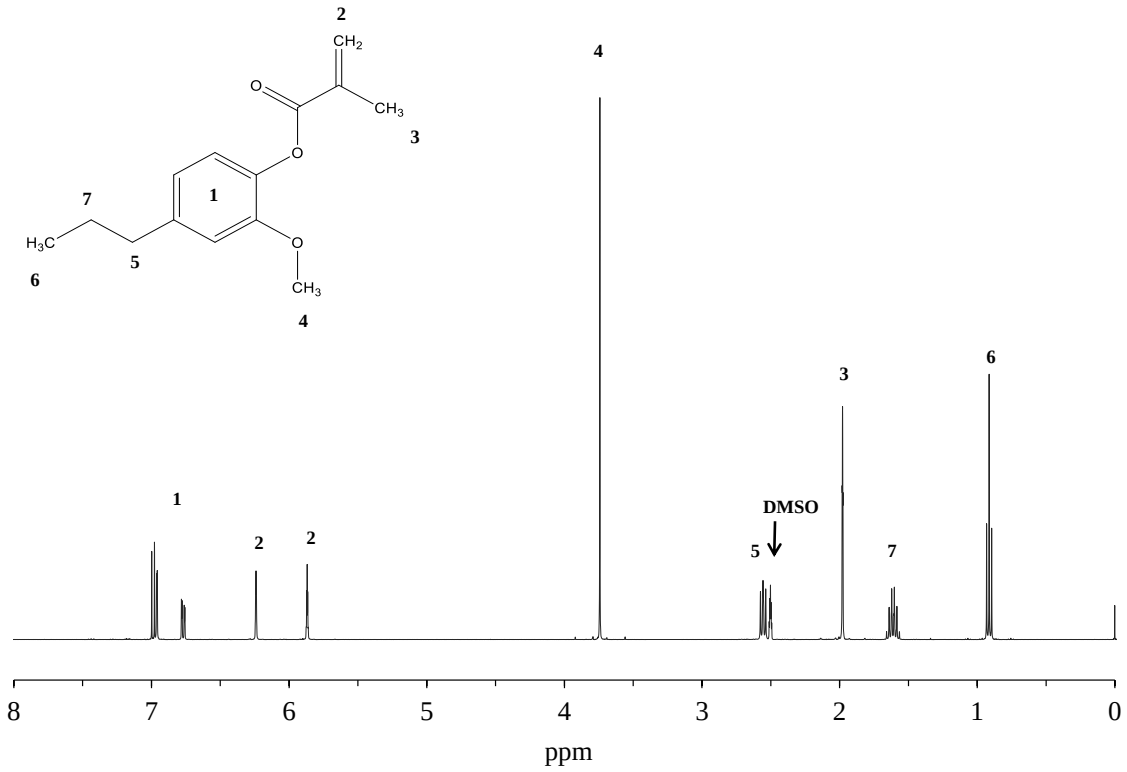

Figure 31. ^{1}H NMR spectra of pure (>97.5 mol %) methacrylated 4-propylguaiacol.

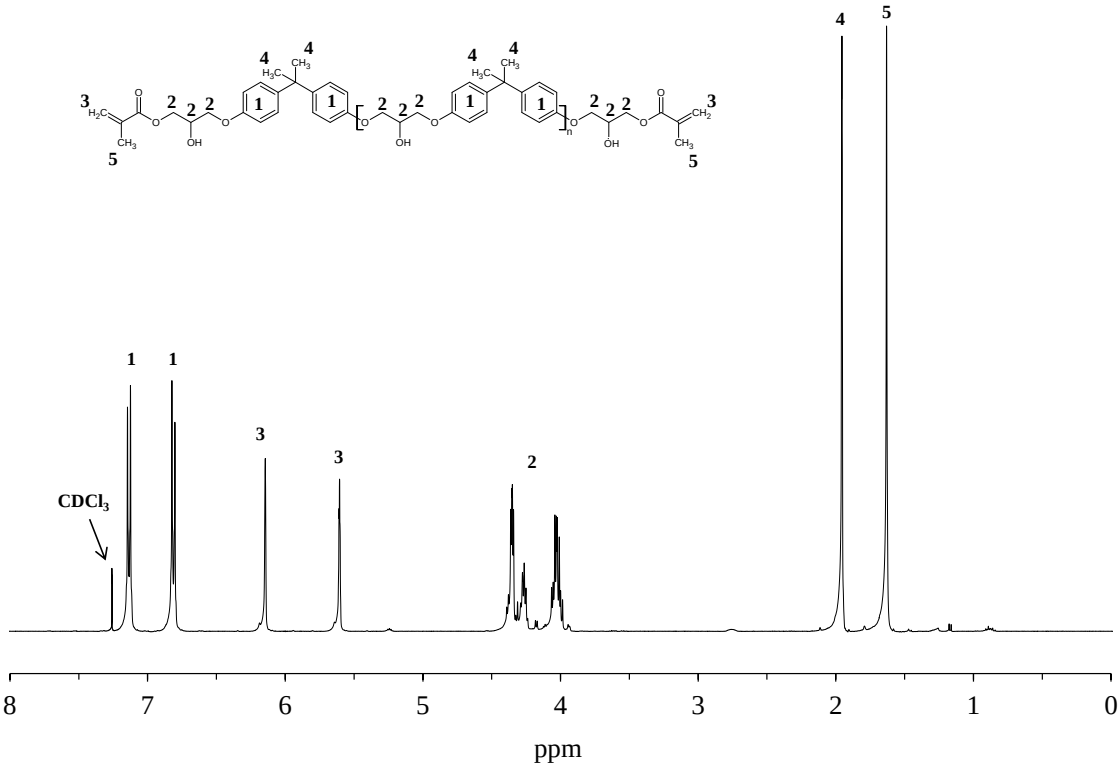

Figure 32: ^{1}H NMR spectra of VE828.

Appendix B

GPC Traces of Pure MLMCs

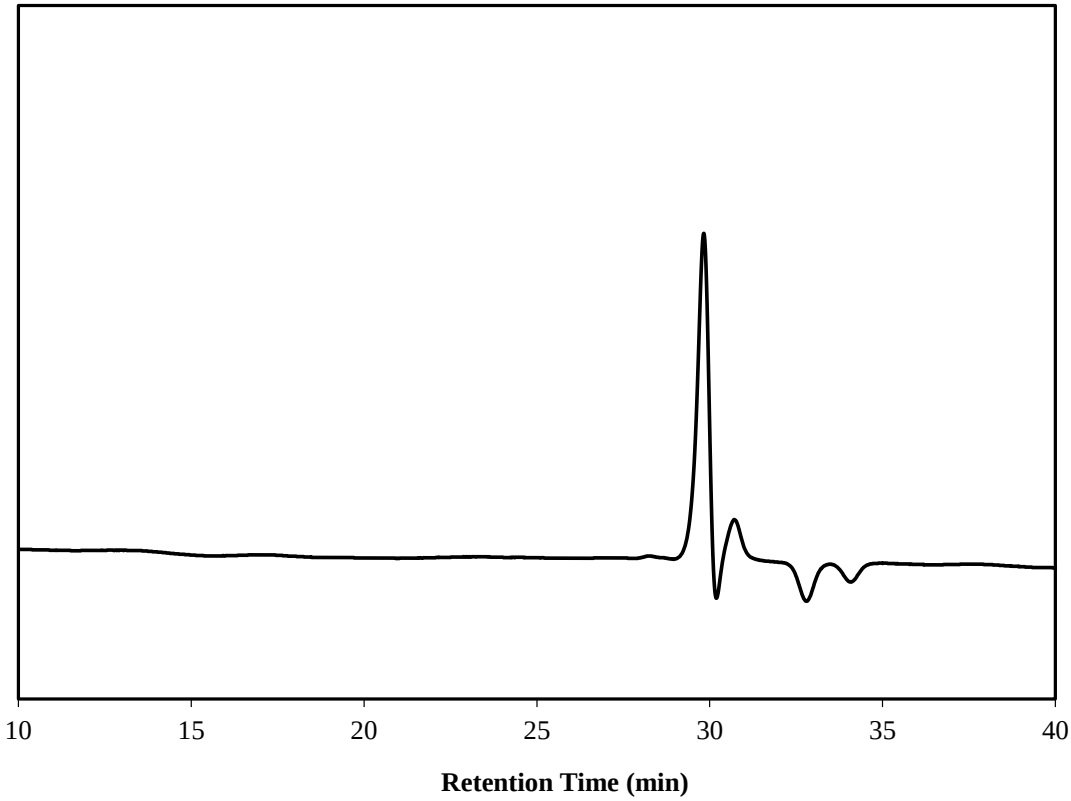

Figure 33. GPC trace of pure (>97.5 mol %) methacrylated phenol.

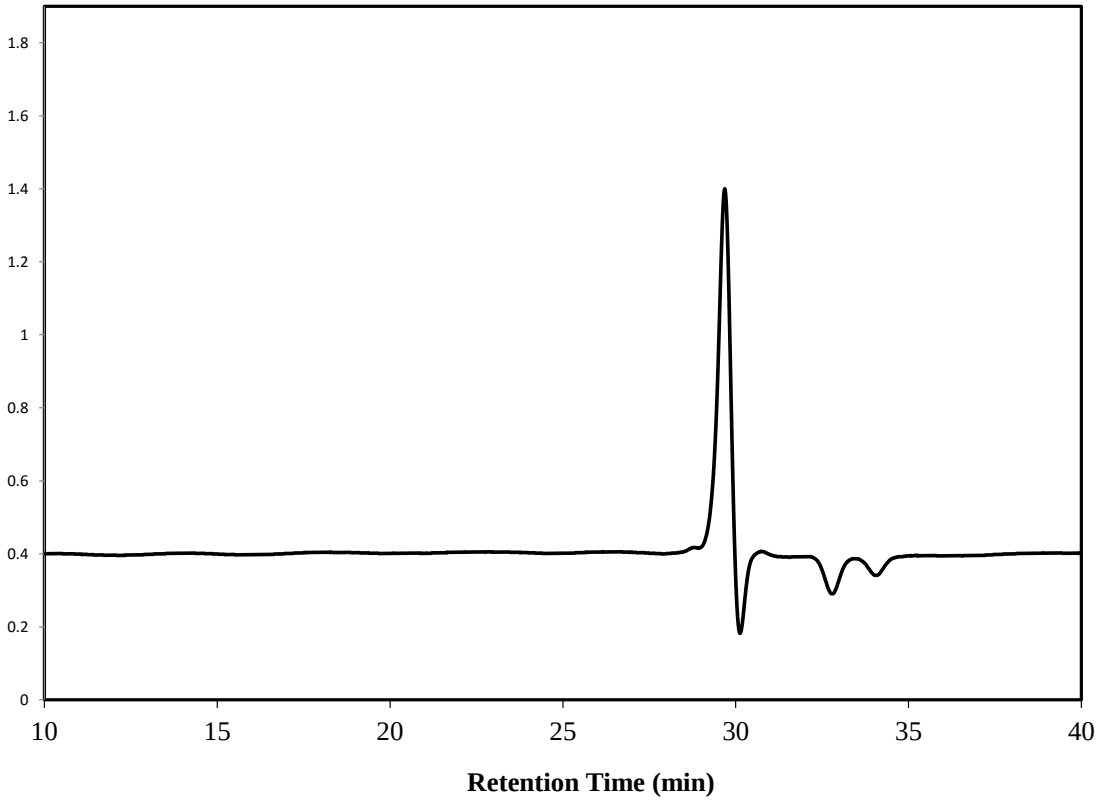

Figure 34. GPC trace of pure (>97.5 mol %) methacrylated guaiacol.

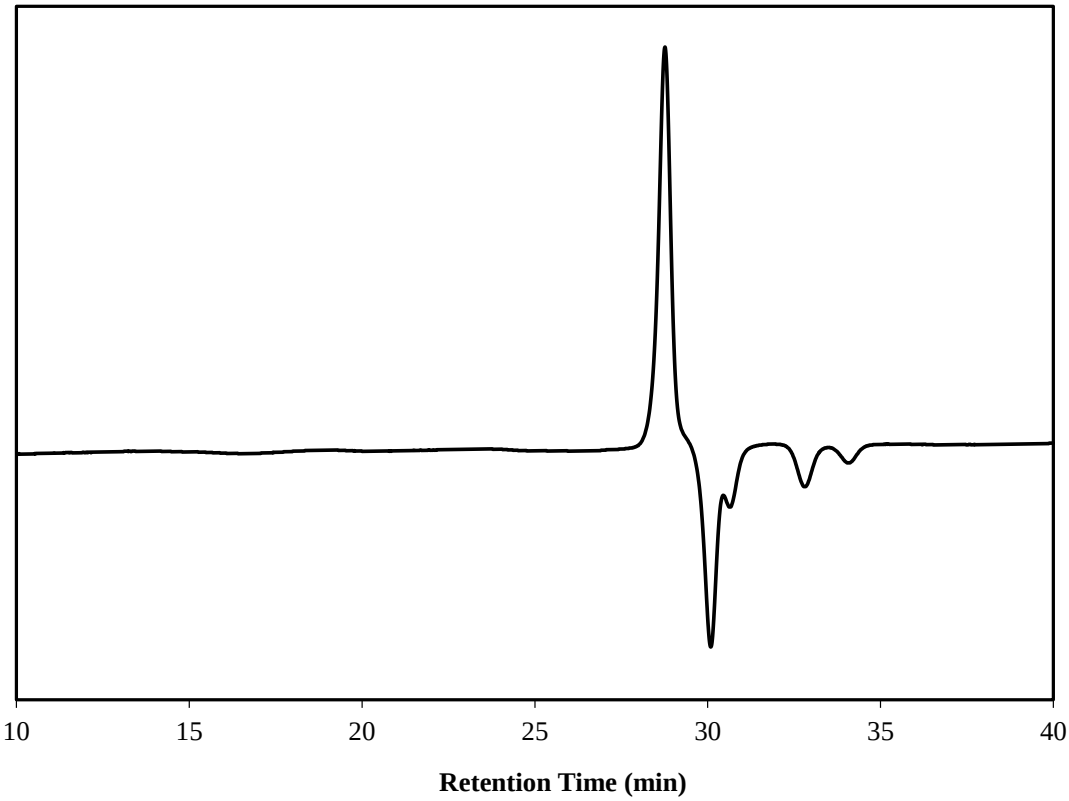

Figure 35. GPC trace of pure (>97.5 mol %) methacrylated 4-propylguaiacol.

Appendix C

GPC Standard Curve

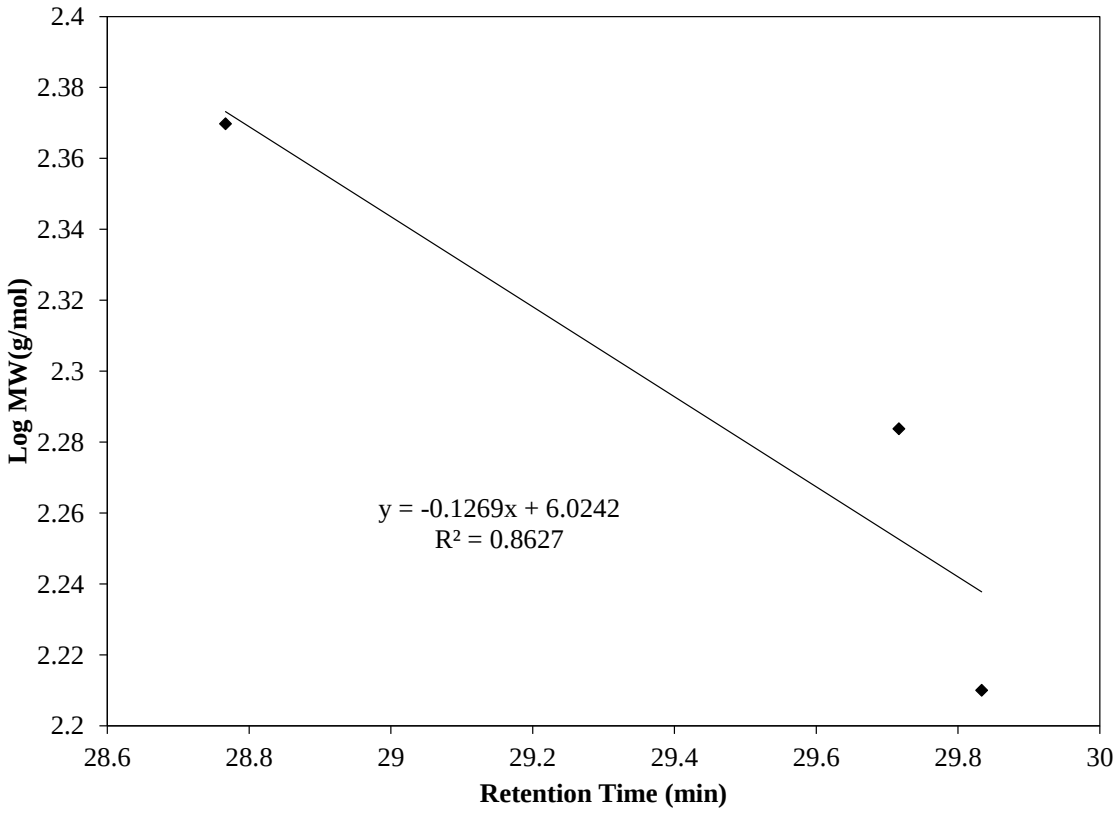

Figure 36. Standard curve generated using the retention times of pure (>97.5 mol %) PM, MG, and M4PG.